nature communications

Article

https://doi.org/10.1038/s41467-024-54997-2

Cell competition drives bronchiolization and pulmonary fibrosis

Received: 29 March 2024

Accepted: 27 November 2024

Published online: 05 December 2024

Check for updates

Rachel Warren[1], Kylie Klinkhammer[1], Handeng Lyu[1], Joseph Knopp[1], Tingting Yuan[2], Changfu Yao[3], Barry Stripp[3] & Stijn P. De Langhe[1]

Idiopathic pulmonary fibrosis (IPF) is a progressive respiratory scarring disease arising from the maladaptive differentiation of lung stem cells into bronchial epithelial cells rather than into alveolar type 1 (AT1) cells, which are responsible for gas exchange. Here, we report that healthy lungs maintain their stem cells through tonic Hippo and β-catenin signaling, which promote Yap/Taz degradation and allow for low-level expression of the Wnt target gene *Myc*. Inactivation of upstream activators of the Hippo pathway in lung stem cells inhibits this tonic β-catenin signaling and *Myc* expression and promotes their Taz-mediated differentiation into AT1 cells. Vice versa, increased Myc in collaboration with Yap promotes the differentiation of lung stem cells along the basal and myoepithelial-like lineages allowing them to invade and bronchiolize the lung parenchyma in a process reminiscent of submucosal gland development. Our findings indicate that stem cells exhibiting the highest Myc levels become supercompetitors that drive remodeling, whereas loser cells with lower Myc levels terminally differentiate into AT1 cells.

Idiopathic pulmonary fibrosis (IPF) pathogenesis encompasses alveolar and fibrotic remodeling, inflammation, and eventual loss of lung architecture[1] resulting in progressive loss of pulmonary function, respiratory failure, and death often within 5 years of diagnosis[2,3]. Accumulating genetic data implicate impaired epithelial maintenance and function as drivers of pulmonary fibrosis[4–8].

The alveolar epithelium is primarily comprised of alveolar type 2 stem cells (AT2s) and alveolar type 1 cells (AT1s) responsible for gas exchange. Club stem cells and AT2 stem cells are capable of self-renewal and differentiation into AT2 and/or AT1 cells through a pre-AT1 transitional cell state (PATS) that has only recently been appreciated[9–11]. Hallmarks of ineffectual repair include the aberrant accumulation of PATS[9,10,12] and ectopic airway differentiation, called bronchiolization, a prominent feature of interstitial lung disease[12–19]. In vivo, there is no evidence for AT2 stem cells and some evidence for Club cells contributing to bronchiolization[20,21]. In fact, upon H1N1 influenza injury, the stem cells driving this bronchiolization have been demonstrated to be intralobular serous cells[22], intralobular airway-resident basal p63+ progenitors[21] and to a limited extent preexisting basal cells (BCs)[23] all of which depend on Trp63. For the purpose of this manuscript, we will group these together as basal-like cells (BLCs). Once established bronchiolization is difficult to resolve and this persistence of bronchial epithelial cells incapable of gas exchange ultimately leads to death. However, genetic interventions have suggested that it may be possible to reprogram these bronchiolized areas into alveolar epithelium and potentially cure this disease[20,24].

Interestingly, whether bronchiolization occurs seems to largely depend on the level of injury, e.g., catastrophic injury to the lung parenchyma which wipes out the majority of AT2s, AT1s and Club cells, suggesting that some form of cell competition may be at play. Indeed, BLCs are resistant to influenza virus[24] and SARS-CoV-2[25] infection. Therefore, one possibility is that BLCs under normal conditions are kept at bay by "more competitive" Club cells or AT2 stem cells. Interestingly, upon Sendai virus infection which only destroys Club cells and AT2 cells but not AT1 cells[26], BLCs have been shown to outcompete

[1]Department of Medicine, Division of Pulmonary and Critical Medicine, Mayo Clinic, Rochester, MN, USA. [2]Department of Medicine, Division of Pulmonary, Allergy & Critical Care Medicine, University of Alabama at Birmingham, Birmingham, AL, USA. [3]Women's Guild Lung Institute, Department of Medicine, Cedars-Sinai Medical Center, Los Angeles, CA, USA. e-mail: delanghe.stijn@mayo.edu

and replace surviving AT1 cells and bronchiolize the lung parenchymal regions devoid of AT2 stem cells[27].

In tissues harboring a mosaic imbalance in Myc protein levels, cells with higher Myc levels expand at the expense of cells with lower levels by eliminating them through apoptosis, inducing senescence, promoting autophagy, or directing them to terminal differentiation and sloughing[28]. Cells measure their Myc content relative to their neighbors, and cells with lower Myc levels are eliminated by neighbors with higher Myc[29,30]. This process is known as cell competition[28,31–35]. Cells that grow faster and eliminate less-fit cells are called super-competitors. Cells become super-competitors when their levels of Myc expression are two-fold higher than that of their neighbors[29,31,36,37]. This process may reflect a selection for fit cells, since Myc maintains stemness, eliminating cells with lower Myc may guard against premature differentiation.

Here, we demonstrate that lung epithelial stem cell competitiveness/fitness levels are determined by their Myc levels, which are tuned by the Hippo pathway. Healthy lungs maintain their stem cells through tonic Hippo and β-catenin signaling, which promote Yap/Taz degradation and allow for low-level expression of the Wnt target gene *Myc*. Inactivation of upstream activators of the Hippo pathway, *Mst1/2* (encoded by *Stk3/4*), in AT2 or Club stem cells stabilizes Taz, which inhibits *Myc* expression by promoting β-catenin degradation and allows for Taz to translocate to the nucleus and drive AT1 cell differentiation. Vice versa, increased Myc in collaboration with Yap promotes the differentiation of lung stem cells along the basal and myoepithelial-like lineages allowing them to invade and bronchiolize the lung parenchyma in a process reminiscent of submucosal gland development. Our findings indicate that stem cells exhibiting the highest Myc levels become supercompetitors that drive remodeling, whereas loser cells with lower Myc levels terminally differentiate into AT1 cells.

Results

Club cells compete with BLCs to regenerate vs bronchiolize the lung parenchyma upon catastrophic injury to the lung parenchyma

After catastrophic injury to the lung parenchyma by influenza infection, bronchial epithelial stem cells (BESCs) in the airway have been proposed to undergo a binary response to reconstitute epithelial barriers giving rise to either alveolar epithelium or generate more airway epithelium and "bronchiolize" the lung parenchyma. However, it has been unclear whether one particular BESC subpopulation undergoes this binary response or whether there is competition between different BESC populations capable of either promoting alveolar epithelial regeneration or bronchiolization. This is largely because most lineage tracing experiments to target BESCs rely on *Sox2^{CreERT2};mTmG* mice which lineage labels all bronchial epithelial cells.

It is well known that subsets of Club cells (e.g., BASCs) can give rise to both airway and alveolar epithelium[38–40] but do not contribute in a significant way to bronchiolization of the lung parenchyma after catastrophic injury mediated by H1N1 influenza[21]. However, because Club cells and especially BASCs are also destroyed by H1N1 influenza it has been difficult to assert whether they can contribute to alveolar epithelial regeneration if they survive the initial injury. To investigate this, we used *Scgb1a1^{CreERT};mTmG* mice to lineage label Club cells, including BASCs and performed H1N1-mediated injury. Our experiments confirm previous reports that Club cells do not participate in the bronchiolization of the lung parenchyma after H1N1-mediated injury (Fig. 1A–D) which is known to be mediated by BLCs under this condition[21]. However, we find that if Club cells survive the initial assault they can contribute to alveolar epithelial regeneration after injury (Fig. 1B–D). Remarkably, Club cells regenerating alveolar epithelium or BLCs bronchiolizing the lung parenchyma are mutually exclusive events i.e. a binary response, suggesting that when Club cells survive the initial assault, they compete with BLCs, preventing them from invading and bronchiolizing the lung parenchyma.

In tissues harboring a mosaic imbalance in Myc protein levels, cells with higher Myc levels expand at the expense of cells with lower levels by eliminating them through apoptosis, inducing senescence, promoting autophagy or directing them to terminal differentiation and sloughing[28]. To investigate whether Club cells compete with BLCs using the classic cell competition model we inactivated *Myc* in Club cells specifically using *Scgb1a1^{CreERT};Myc$^{f/f}$;mTmG* mice while simultaneously lineage tracing them. We find that upon H1N1 injury alveolar epithelial regeneration by Club cells in *Scgb1a1^{CreERT};Myc$^{f/f}$;mTmG* mice is impaired with the majority being outcompeted by BLCs (Fig. 1E–L) and the remainder giving rise preferentially to AT1 rather than AT2 cells compared to *Scgb1a1^{CreERT};mTmG* control mice, that feature normal Myc levels. *Scgb1a1^{CreERT};Myc$^{f/f}$;mTmG* lungs featured increased bronchiolization mediated by BLCs (Fig. 1E, I, L) and increased pulmonary fibrosis as measured by hydroxyproline content (Fig. 1K). Together these findings indicate that stem cell competition in the lung is governed by Myc levels.

Subsets of bronchial epithelial stem cells acquire myoepithelial cell characteristics after injury to the lung parenchyma

We next wanted to investigate how Myc levels in BLCs affect bronchiolization. To do this we performed immunostaining for Myc on lungs after H1N1 injury or severe bleomycin injury. We show that after catastrophic H1N1 or severe bleomycin injury some BESC offspring at the periphery or leading edge of the BC-pods feature high Myc levels (Fig. 2A–C, Supplementary Fig. 1A–H). Interestingly, these leading edge BLCs unlike trailing cells in the BC pods also express high levels of Sox9 and Acta2 (Fig. 2D, E), reminiscent of myoepithelial cells (MECs) in the submucosal gland[41,42] (SMG). Immunostaining and scRNAseq analysis of human IPF tissue demonstrate that subsets of BCs in honeycomb cysts of IPF lungs also feature high levels of Myc, Sox9 and/or Acta2 expression reminiscent of myoepithelial cells present in microdissected proximal airways of human donors confirming the proximalization of human IPF containing myoepithelial-like cells in the distal epithelium (Fig. 2F, G, Supplementary Fig. 1I–M).

To investigate if the MEC-like cells at the leading edge of the BC pods are derived from MECs in the SMG, we lineage labeled the latter prior to injury using a *Nkx2.1^{Flpo};Acta2-Frt-STOP-Frt-CreERT2;mTmG*[43] intersectional mouse model in which we can specifically lineage label lung epithelial cells that co-express the lung epithelial cell marker Nkx2.1 and the mesenchymal Acta2 (α-SMA) marker. The *Acta2-Frt-STOP-Frt-CreERT2* knock-in mouse line, possesses a CreERT2 cassette, inserted in the *Acta2* locus, which is preceded by a STOP codon, flanked by Frt sites. As such, when crossed with *Nkx2.1^{Flpo}* expressing mice, *Acta2-Frt-STOP-Frt-CreERT2* mice permanently express *CreERT2* in *Acta2* and *Nkx2.1^{Flpo}* co-expressing cells as well as their offspring, due to removal of the STOP codon. This then allows for the lineage labeling of MECs in *Nkx2.1^{Flpo};Acta2-Frt-STOP-Frt-CreERT2;mTmG* after tamoxifen treatment.

Using this mouse model we find that SMG MECs do not migrate and give rise to BC pods after H1N1 injury (Fig. 3A, B). However, we can label de novo myoepithelial like cells in BC-pods by treating this same intersectional mouse model with tamoxifen after H1N1 injury (Fig. 3C, D), suggesting that BLCs, other than the MECs in the SMG, can acquire MEC-like characteristics upon catastrophic H1N1 or bleomycin injury. We were able to confirm these findings using two additional intersectional mouse models *Trp63^{DreERT2};Acta2^{CreERT2};RLTG* and *Nkx2.1^{Flpo}; Acta2^{CreERT2};FLTG* (Fig. 3E, G–L).

Using *Trp63^{DreERT2};Acta2^{CreERT2};RLTG* we can specifically target MEC-like cells that co-express the basal cell transcription factor *Trp63* and the mesenchymal *Acta2* (α-SMA) marker. Tamoxifen exposure results in Dre-mediated excision of a polyA signal (STOP) from the RLTG dual recombinase reporter allele (Dre/Cre recombinase reporter) within

Trp63 expressing intralobular basal cells, with subsequent Cre-mediated excision of *tdTomato-STOP* within *Acta2*-expressing MECs. Outcomes of these recombination events include tracing of *Trp63*$^{+}$-intralobular basal cells by expression of *tdTomato*, and *Trp63*$^{+}$/*Acta2*$^{+}$ MECs by expression of eGFP (Fig. 3E).

Using *Nkx2.1*^{Flpo}; *Acta2*^{CreERT2};*FLTG* we can specifically target MEC-like cells that co-express the lung epithelial-specific transcription factor *Nkx2.1* and the mesenchymal *Acta2* (α-SMA) marker. Flpo-mediated excision of a polyA signal (STOP) from the FLTG dual recombinase reporter allele (Flpo/Cre recombinase reporter) occurs within *Nkx2.1* expressing lung epithelial cells, with subsequent tamoxifen-induced Cre-mediated excision of tdT-STOP within *Acta2*-expressing MEC like cells. Outcomes of these recombination events include tracing of *Nkx2.1*$^{+}$-lung epithelial cells by expression of *tdTomato*, and *Nkx2.1*$^{+}$/*Acta2*$^{+}$ myoepithelial-like cells by expression of eGFP (Fig. 3G–L).

Finally, to investigate whether all cells in BC pods may be derived from these MEC like cells that lead the invasion we gave tamoxifen chow to *Sox9*^{CreERT2};*mTmG* mice after H1N1 injury and found that all cells in the BC pods were lineage labeled (Fig. 3F), indicating that all cells in basal cell pods either induced *Sox9* expression at some point during the invasion of BC pods or are all derived from the MEC-like stem cells at the leading edge of the invasion. Indeed, treating *Nkx2.1*^{Flpo}; *Acta2*^{CreERT2};*FLTG* mice with tamoxifen 2 weeks after H1N1 injury, lineage labels MEC-like cells and their offspring and demonstrates that myoepithelial-like cells do differentiate into conducting airway epithelial cells such as Dclk1^{+} tuft cells (Fig. 3I), Foxj1^{+} ciliated cells (Fig. 3J) and Scgb1a1^{+} club cells (Fig. 3K, L). This is interesting as it indicates that super-competitor myoepithelial like cells may give rise to all trailing cells in the basal cell pods. Our findings further suggest that the process of bronchiolization is reminiscent of the process that drives

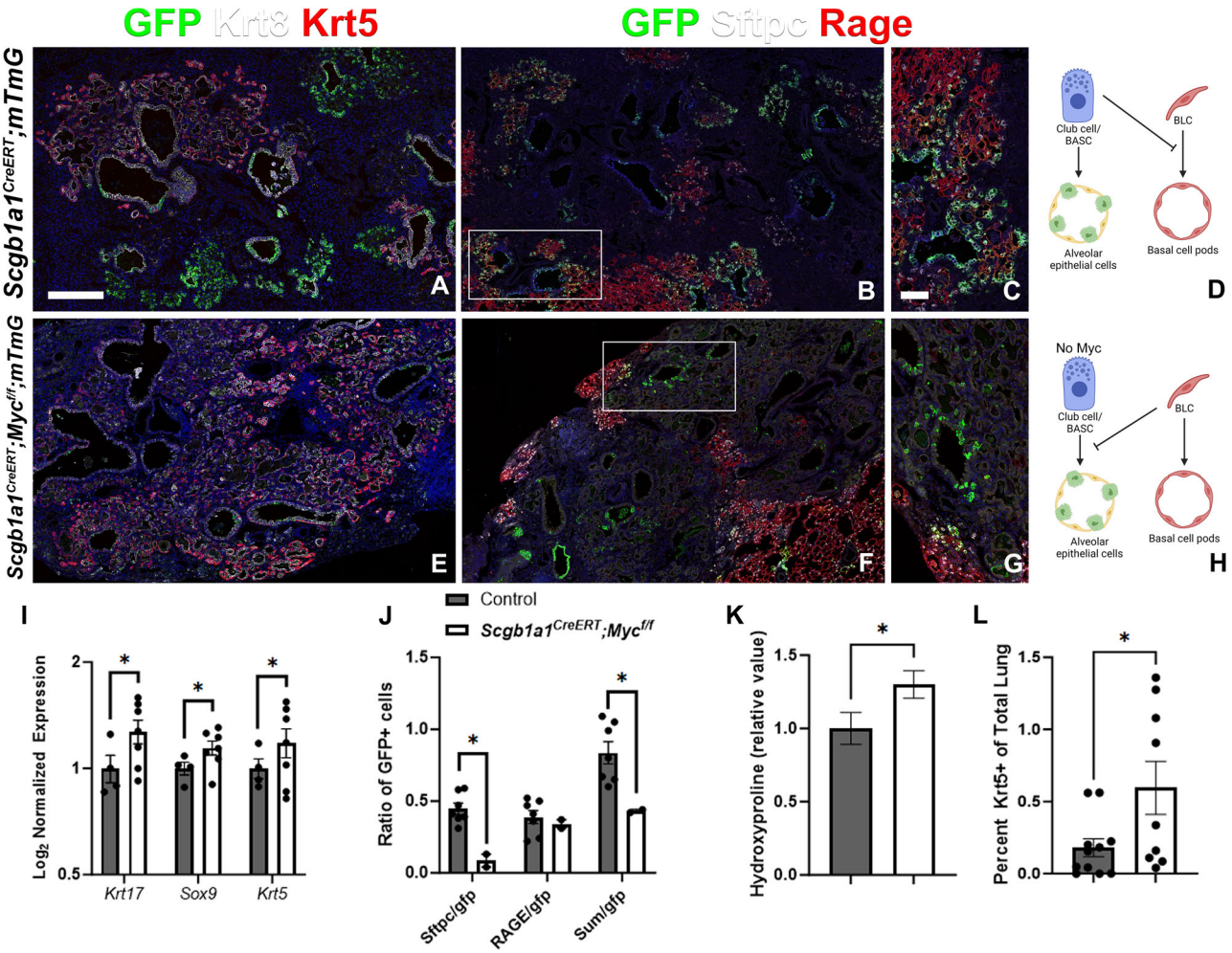

Fig. 1 | Club cells compete with BLCs to regenerate vs bronchiolize the lung parenchyma upon catastrophic injury to the lung parenchyma. *Scgb1a1*^{CreERT};*mTmG* and *Scgb1a1*^{CreERT};*Myc*$^{f/f}$;*mTmG* were placed on tamoxifen containing chow at 8 weeks of age for 3 weeks to inactivate *Myc* and permanently label all Club cells/BASCs and their offspring with GFP. After a 3 week wash-out period, mice were infected with H1N1 influenza virus, and lungs were harvested at 6 weeks post injury. Coimmunostaining for GFP (lineage label), Keratin 5 (Krt5; basal and BLCs), and Keratin 8 (Krt8; BLCs and transitional cells) on *Scgb1a1*^{CreERT};*mTmG* (**A**) and *Scgb1a1*^{CreERT};*Myc*$^{f/f}$;*mTmG* (**E**) lung sections. Coimmunostaining for GFP (lineage label), surfactant protein C (Sftpc; AT2 cells), Rage (AT1 cells) on *Scgb1a1*^{CreERT};*mTmG* (**B**, **C**) and *Scgb1a1*^{CreERT};*Myc*$^{f/f}$;*mTmG* (**F**, **G**) lung sections. White boxes in **B** and **F** are enlarged in (**C**, **G**), respectively. **D** Diagram demonstrating that normal Club cells inhibit BLCs and give rise to alveolar epithelial cells. **H** Diagram demonstrating that Myc deficient Club cells are outcompeted by Myc sufficient BLCs. Created in BioRender. Warren (2024) https://BioRender.com/ k46i357. **I** Nanostring nCounter analysis on RNA from *Scgb1a1*^{CreERT};*mTmG* ($n = 4$) and *Scgb1a1*^{CreERT};*Myc*$^{f/f}$;*mTmG* ($n = 7$) lungs for BLC genes *Keratin 17* ($p = 0.03$, Log2 fold change = −1.87), *Sox9* ($p = 0.03$, Log2 fold change = −1.04), and *Krt5* ($p = 0.047$, Log2 fold change = −1.86). Data are Log2 normalized. **J** Lineage tracing analysis on immunostaining in **B** ($n = 7$), E ($n = 2$) using Aivia machine learning software (Sftpc/gfp $p = 0.003$, RAGE/gfp $p = 0.6$, Sum/gfp $p = 0.03$). **K** Hydroxyproline analysis on *Cre*- controls ($n = 17$) and *Scgb1a1*^{CreERT};*Myc*$^{f/f}$;*mTmG* ($n = 20$) lungs normalized to control ($p = 0.04$). **L** Image analysis of total area of basal cells in control ($n = 11$) and *Scgb1a1*^{CreERT};*Myc*$^{f/f}$;*mTmG* ($n = 9$) lung sections ($p = 0.03$). Data are presented as mean values +/− SEM. Scale bar: 250 µm. Two two-tailed unpaired T-test was used to determine significance. F test was used to determine equal variances and unreported F values indicate equal variance. $^{*}p < 0.05$, $^{**}p < 0.01$.

https://doi.org/10.1038/s41467-024-54997-2

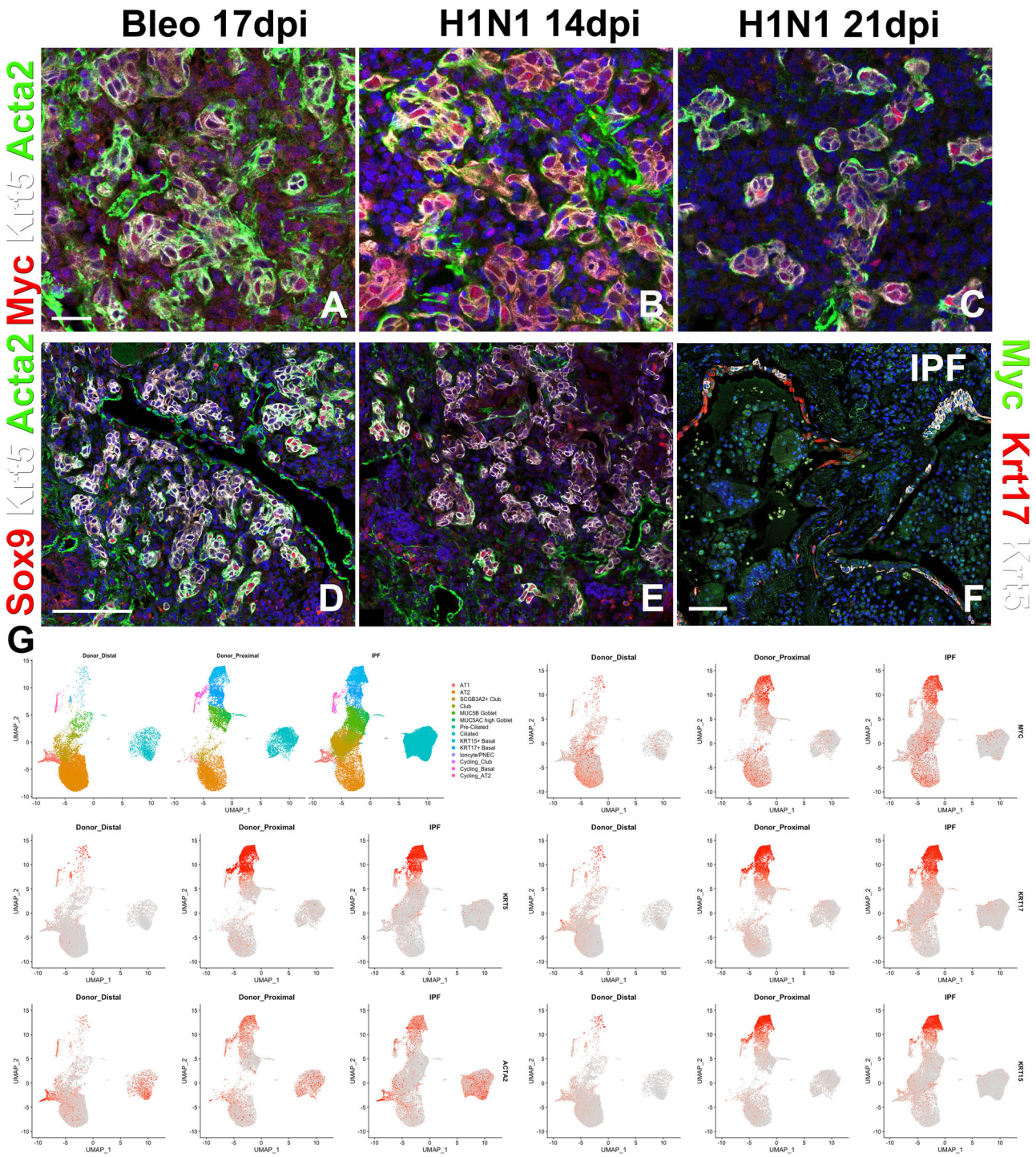

Fig. 2 | High expression of *Myc* in BLCs in IPF. A–E Coimmunostaining for myoepithelial cell markers Myc (**A**–**C**) or Sox9 (**D**, **E**), Krt5, and Acta2 (smooth muscle actin) on honeycomb regions in mouse lungs 17 days after bleomycin (**A**–**D**) and 14 or 21 days after H1N1 injury (**B**, **C**, **E**). **F** Coimmunostaining for Myc, Krt17, and Krt5 on honeycomb regions in human IPF tissue. (**G**) scRNAseq analysis of myoepithelial cell genes *Krt5*, *Krt17, Myc*, and *Acta2* expression in human IPF vs donor lungs. Uniform Manifold Approximation and Projection (UMAP) of 10x scRNAseq data on human control (Donor Distal) and control including microdissected proximal airways (donor proximal) and IPF distal lungs demonstrating high Myc, Krt5, Krt17, Krt15, Acta2 expression in bronchiolized epithelium in IPF and proximal airway basal cells. Scale bar: 50 µm (**A**–**C**), 100 µm (**D**–**F**).

submucosal gland development, suggesting that BC pods may be considered as de novo submucosal glands[44,45].

Myc drives bronchiolization and fibrosis through the generation of myoepithelial-like cells

To investigate if Myc levels in BESCs affect stem cell competition after severe bleomycin or H1N1 injury we generated *Sox2*^{CreERT2};*Myc*$^{f/f}$;*mTmG* mice in which we can inactivate *Myc* in all BESCs, in order to level fitness levels, while simultaneously lineage labeling them. When we perform bleomycin (Fig. 4B–K) or H1N1 (Fig. 4L–U) injury on *Sox2*^{CreERT2};*Myc*$^{f/f}$;*mTmG* mice, in which we inactivated *Myc* in BESCs prior to injury (Fig. 4A), BESCs fail to acquire MEC-status and fail to bronchiolize the lung parenchyma, as demonstrated by impaired basal cell pod generation (Fig. 4B, E, K, L, O, U) and reduced expression of

https://doi.org/10.1038/s41467-024-54997-2

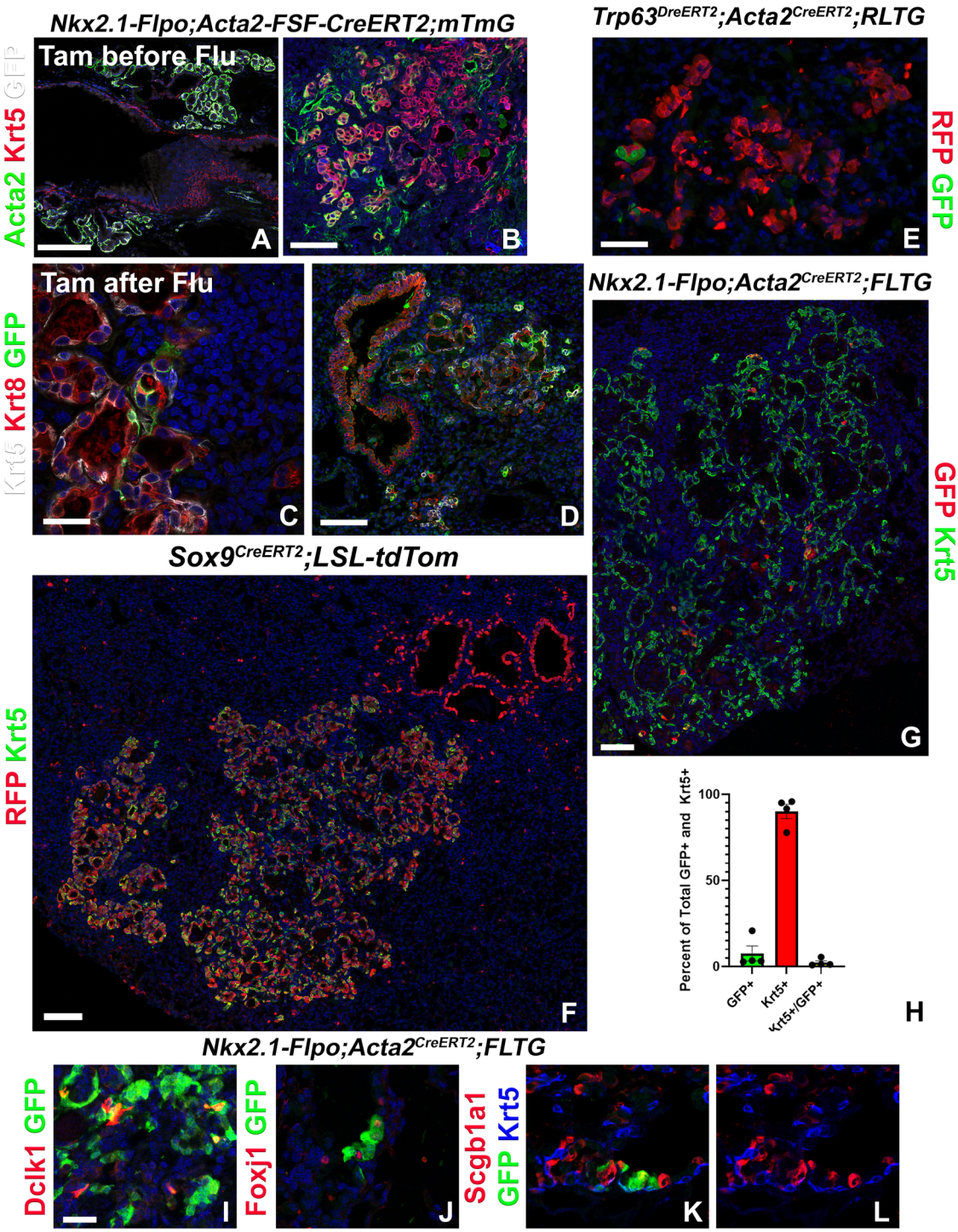

Fig. 3 | Basal cell pod development resembles submucosal gland development. **A**, **B** *Nkx2.1*^{Flpo};*Acta2-Frt-STOP-Frt*^{CreERT2};*mTmG* mice were place on tamoxifen containing chow for 3 weeks. Following a 3 week washout period, mice were infected with H1N1. At 6 weeks after injury, left lung lobes and trachea were inflation fixed, embedded in paraffin, and sectioned. Coimmunostaining for myoepithelial cell markers Acta2, Krt5, and lineage label GFP on *Nkx2.1*^{Flpo};*Acta2-Frt-STOP-Frt*^{CreERT2};*mTmG* trachea (**E**) and lung (**F**). **C**, **D** *Nkx2.1*^{Flpo};*Acta2-Frt-STOP-Frt*^{CreERT2};*mTmG* mice were intranasally administered H1N1. At 2 weeks after injury mice were placed on tamoxifen containing chow. At 6 weeks after injury, left lung lobes and trachea were inflation fixed, embedded in paraffin, and sectioned. Coimmunostaining for Krt5, Krt8, and GFP on *Nkx2.1*^{Flpo};*Acta2-Frt-STOP-Frt*^{CreERT2};*mTmG* lungs. **E** *Trp63*^{DreERT2};*Acta2*^{CreERT2};*RLTG* mice were intranasally administered H1N1 and placed on tamoxifen containing chow at 2 weeks after injury. tdTomato is induced in only *Trp63*^{DreERT2} expressing cells and GFP is induced only when both Trp63^{DreERT2} and *Acta2*^{CreERT2} are expressed (myoepithelial cells). Coimmunostaining for RFP (tdtomato) and GFP on lungs at 6 weeks after injury. **F** *Sox9*^{CreERT2};*tdTomato* mice were intranasally administered H1N1 and placed on tamoxifen containing chow at the injury. Coimmunostaining for RFP (tdTomato) and Krt5 on lungs at 6 weeks after injury. **G**–**L** *Nkx2.1*^{Flpo}; *Acta2*^{CreERT2};*FLTG* mice were intranasally administered H1N1 and placed on tamoxifen containing chow at 2 weeks after injury with additional tamoxifen shots at 14 and 16 days after injury. tdTomato is induced in only *Nkx2.1*^{Flpo} expressing cells and GFP is induced only when both *Nkx2.1*^{Flpo} and *Acta2*^{CreERT2} are expressed (myoepithelial cells). **G** Coimmunostaining for GFP and Krt5 on lungs at 6 weeks after injury and (**H**) image analysis using Aivia machine learning software ($n = 4$ animals). Coimmunostaining for GFP and (**I**) Dclk1 (tuft cells), (**J**) Foxj1 (ciliated cells), and (**K**, **L**) Scgb1a1 (secretory cells) and Krt5 (BLCs). Data are presented as mean values +/− SEM. Scale bar: 200 µm (**A**) 100 µm (**D**, **F**), 50 µm (**B**, **G**), 25 µm (**C**, **E**, **I**–**L**).

https://doi.org/10.1038/s41467-024-54997-2

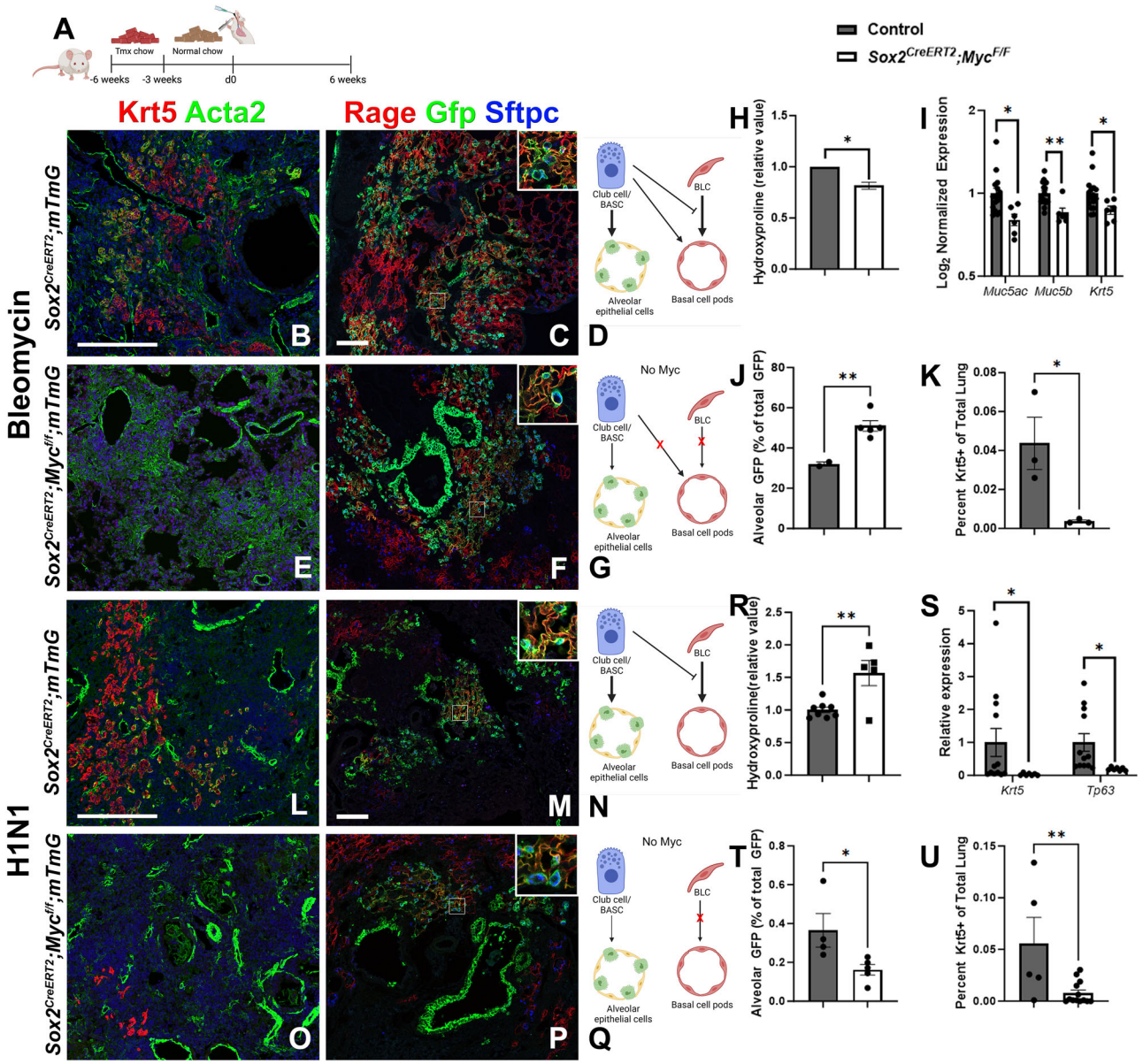

Fig. 4 | Airway epithelial Myc is required for bronchiolization. A Mice were placed on tamoxifen chow for 3 weeks to inactivate Myc and permanently lineage label bronchial epithelial cells and their offspring. Following a 3-week washout period, mice were injured with intratracheal administration of bleomycin (**B**–**K**) or intranasal administration of H1N1 (**L**–**U**) and lungs were harvested at 6 weeks post injury. (**B**, **E**, **L**, **O**) Immunostaining for Krt5 (basal and BLCs) and Acta2 (smooth muscle actin; myofibroblasts) on bleomycin (**B**, **E**) and influenza (**L**, **O**) injured *Sox2*^{CreERT2}*;mTmG* and *Sox2*^{CreERT2}*;Myc*$^{f/f}$*;mTmG*. (**C**, **F**, **M**, **P**) Immunostaining for Rage (AT1 cells), GFP (lineage label), and Sftpc (AT2 cells) on *Sox2*^{CreERT2}*;mTmG* and *Sox2*^{CreERT2}*;Myc*$^{f/f}$*;mTmG*. (**D**, **G**, **N**, **Q**) Models demonstrating that Myc sufficient Club cells inhibit BLCs and give rise to alveolar epithelial cells after bleomycin (**D**) and influenza (**N**) injury but Myc insufficient BLCs fail to give rise to basal cell pods (**G**, **Q**). Created in BioRender. Warren (2024) https://BioRender.com/j04r129. **H** Hydroxyproline analysis on bleomycin injured *Cre-* controls ($n = 26$) and *Sox2*^{CreERT2}*;Myc*$^{f/f}$ ($n = 19$) ($p = 0.04$). **I** Nanostring nCounter analysis on RNA from bleomycin injured *Cre-* controls ($n = 17$) and *Sox2*^{CreERT2}*;Myc*$^{f/f}$*;mTmG* ($n = 6$) lungs BLC genes (*Muc5ac* $p = 0.01$, *Muc5b* $p = 0.003$, *Krt5* $p = 0.046$). Data are Log2 normalized. **J** Lineage tracing analysis on bleomycin injured lungs from immunostaining in (**C**) ($n = 2$), (**F**) ($n = 5$) using Aivia machine learning software ($p = 0.008$). **K** Image analysis of the total area of basal cells in bleomycin injured control (n = 3) and *Sox2*^{CreERT2}*;Myc*$^{f/f}$*;mTmG* ($n = 3$) lung sections ($p = 0.04$). **R** Hydroxyproline analysis on influenza injured *Cre-* controls ($n = 8$) and *Sox2*^{CreERT2}*;Myc*$^{f/f}$ ($n = 5$) ($p = 0.004$). **S** qPCR analysis on RNA from influenza injured *Cre-* controls ($n = 12$) and *Sox2*^{CreERT2}*;Myc*$^{f/f}$*;mTmG* ($n = 7$) lungs for BLC genes (*Krt5* ($p = 0.04$, $F = 3.32\times10^{-9}$) and *Tp63* ($p = 0.01$, $F = 6.29\times10^{-8}$)). **T** Lineage tracing analysis on influenza-injured lungs from immunostaining in **M** (n = 4), (**P**) ($n = 5$) using Aivia machine learning software ($p = 0.04$). **U** Image analysis of total area of basal cells in influenza injured control ($n = 5$) and *Sox2*^{CreERT2}*;Myc*$^{f/f}$*;mTmG* ($n = 13$) lung sections ($p = 0.007$). Data are presented as mean values +/− SEM. Scale bars: 100 μm. Magnification insets are 400x larger. Two tailed unpaired T-test was used to determine significance. *F* test was used to determine equal variances and unreported F values indicate equal variance. $^{*}p < 0.05$, $^{**}p < 0.01$.

bronchial epithelial markers *Muc5b, Muc5ac* and *Krt5* by Nanostring nCounter RNA analysis (Fig. 4I), qPCR analysis (Fig. 4S) and 10x Visium spatial transcriptomics (Supplementary Fig. 2). Interestingly, BESCs in *Sox2*^{CreERT2}*;Myc*$^{f/f}$*;mTmG* lungs, presumably Club cells/BASCs, give rise to more alveolar epithelium after severe bleomycin injury (Fig. 4C, D, F, G, J) but less alveolar epithelium after H1N1 injury (Fig. 4M, N, P, Q, T) compared to control mice. This is likely because inactivation of *Myc* in Club cells prevents them from giving rise to basal cells and allowing them only to give rise to alveolar epithelium after bleomycin injury resulting in a net increase in regeneration, whereas decreasing Club

cell fitness through *Myc* inactivation likely also makes them more vulnerable to H1N1 infection. As a corollary, *Sox2*^{CreERT2};*Myc*$^{f/f}$;*mTmG* lungs feature reduced pulmonary fibrosis based on hydroxyproline content (Fig. 4H) after bleomycin injury, but increased pulmonary fibrosis after H1N1 injury (Fig. 4R). However, in the H1N1 injury model in which most BASCs and AT2 stem cells are destroyed we find that that the inability of BLCs to robustly participate in the immediate regenerative response, even though maladaptive, is detrimental to survival (Supplementary Fig. 6I) and likely contributes to the increased pulmonary fibrosis (Fig. 4R) compared to littermate controls. Our theory is that de novo submucosal gland development (basal cell pod development) near terminal bronchioles and lung parenchyma that have been catastrophically damaged, is a way to seal off or plug those damaged conducting airways preventing more air from entering the lung via that route, which would cause further mechanical damage to the lung parenchyma.

Inactivation of *Myc* in basal cell pods post H1N1 injury promotes their differentiation into AT1 cells

So far, our findings suggest that Myc levels in lung stem cells determine their fitness levels and that cells with the lowest Myc levels differentiate into AT1 cells. Since BC-pods are known to persist in the lung long after H1N1 infection, we wondered whether *Myc* is required for their maintenance and/or expansion post H1N1 injury. To investigate this we infected *Krt5*^{CreERT2};*mTmG* and *Krt5*^{CreERT2};*Myc*$^{f/f}$;*mTmG* mice with H1N1 influenza, and lineage labeled their BLCs with or without simultaneous inactivation of *Myc*, starting at 2 weeks after injury (Fig. 5C). Interestingly, we find that upon inactivation of *Myc* in BC pods in *Krt5*^{CreERT2};*Myc*$^{f/f}$;*mTmG* mice, BC-pods are reduced in size, as indicated by less GFP RNA per Krt5 transcript, and fewer basal cells in *Krt5*^{CreERT2};*Myc*$^{f/f}$;*mTmG* lung sections (Fig. 5A, B, F) compared to H1N1 injured *Krt5*^{CreERT2};*mTmG* control mice. In addition, we find that compared to H1N1 injured *Krt5*^{CreERT2};*mTmG* mice, fibrosis is reduced in *Krt5*^{CreERT2};*Myc*$^{f/f}$;*mTmG* mice, in which we inactivated *Myc* in BLCs and myoepithelial-like cells after injury (Fig. 5G). More strikingly we find that inactivation of *Myc* in BC pods post H1N1 injury affects BC stem cell maintenance over time and allows for their differentiation towards the AT1 lineage by 12 weeks after H1N1 injury (Fig. 5I–Q).

Overexpression of *Myc* endows subsets of BESCs with a super competitor myoepithelial like status which can outcompete AT2 stem cells

We next wondered what would happen if we boosted the fitness of Club cells by overexpressing *Myc* in Club cells after a less severe bleomycin injury. Overexpression of a dominant active version of the Hippo transcriptional effector *Yap1*^{S112A} in Club cells has been shown to direct their differentiation along the BLC lineages[46], and Myc and Yap have both been shown to be important for cell competition[29,31,36,47,48].

Interestingly, when we overexpress *Myc* in Club cells/BASCs after bleomycin injury (Fig. 6A), Club cells/BASCs massively acquire a super-competitor myoepithelial cell (SCMC) like status, coexpressing Krt5, Acta2, Sox9 and Myc (Fig. 6B–M), resulting in the hyper-invasion and apparent destruction of the lung parenchyma including AT2 cells and its replacement with bronchial epithelial cells demonstrated by increased expression of bronchial epithelial markers *Krt5, Krt17*, and *Muc5b*, increased pulmonary fibrosis based on hydroxyproline content and reduced expression of alveolar epithelial marker *Sftpc* by Nanostring nCounter RNA analysis (Fig. 6B–P) and 10x Visium spatial transcriptomics (Supplementary Fig. 3). This suggests that the cell competition program may converge onto a SCMC plastic like state that can be acquired by different BESC populations.

Lung epithelial stem cell fitness levels are determined by their Myc levels, which are tuned by the Hippo pathway

It is well known that Hippo pathway plays an important role in cell competition, and Yap and Myc are thought to work together in this process[29,31,36,47,48]. It is also well known that *Myc* is a quintessential target gene of the canonical Wnt signaling pathway[49] and that the Hippo pathway controls β-catenin stabilization and nuclear localization[50,51]. However, how the Hippo pathway affects Myc levels seems to be context dependent.

Interestingly, the Hippo pathway is active in AT2[52] and Club cells, demonstrated by Merlin expression, phospho-Yap and phospo-Mst1/2 staining (Supplementary Fig. 5A–E), resulting in the degradation and cytoplasmic retention of Yap and Taz the nuclear effectors of the pathway. To investigate how increased Yap and/or Taz levels may affect *Myc* expression in BESCs cells we inactivated the Hippo kinases *Mst1/2* (encoded by *Stk4/3*) in BESCs, and found that this resulted in decreased *Myc* expression, decreased bronchiolization, increased AT1 cell regeneration and reduced pulmonary fibrosis based on hydroxyproline content upon severe bleomycin injury (Fig. 7A–E, L, N, O, Supplementary Fig. 4). Interestingly, inactivation of the Hippo pathway via deletion of *Nf2* in Club cells or AT2 stem cells in the absence of injury is sufficient to drive their spontaneous differentiation into AT1 cells, consistent with previous reports[53,54] (Supplementary Fig. 5F, G & 8A–H, Q).

To investigate how decreased Yap/Taz levels may affect *Myc* expression in BESCs, we inactivated *Yap1* and *Wwtr1* in BESCs, using *Sox2*^{CreERT2};*Yap1*$^{f/f}$;*Wwtr1*$^{f/f}$;*mTmG* mice, and found that this resulted in increased *Myc* expression, decreased AT1 cell regeneration and increased pulmonary fibrosis based on hydroxyproline content upon severe bleomycin injury (Fig. 7J, K, M–O). Even though *Sox2*^{CreERT2};*Yap1*$^{f/f}$;*Wwtr1*$^{f/f}$;*mTmG* mice feature increased *Myc* levels, their lack of Yap prevents them from BLC-mediated bronchiolization (Fig. 7F, J, K, O). Instead, *Sox2*^{CreERT2};*Yap1*$^{f/f}$;*Wwtr1*$^{f/f}$;*mTmG* mice featured increased goblet cell differentiation based on *Muc5b* expression (Fig. 7O), something we also observed in the absence of injury (Supplementary Fig. 5H, I, L), and which is consistent with previous reports[55] demonstrating the spontaneous differentiation of BESCs into goblet cells upon simultaneous inactivation of *Yap1* and *Wwtr1*.

Together these findings suggest that the Hippo pathway controls Myc levels and therefore stem cell competitiveness by controlling Yap and/or Taz levels. This is consistent with a role for cytoplasmic Taz inhibiting Wnt/β-catenin signaling[50,51]. Interestingly, overexpression of a dominant active *β-catenin* in the airway epithelium has been shown to result in excessive goblet cell differentiation[56].

Yap-Myc-p63 promote bronchiolization whereas Taz promotes AT1 differentiation

The fact that inactivation of upstream Hippo kinases (*Nf2, Stk3/4, Lats1/2*) in Club[57] (Supplementary Fig. 6F, G) or AT2 (Fig. 8A–H)[52] cells results in their spontaneous differentiation into AT1 cells is intriguing since we and others have previously demonstrated that Yap is required for tracheal BC maintenance[46,58] and overexpression of a dominant active version of the Hippo transcriptional effector *Yap1*^{S112A} in Club cells is able to drive their differentiation towards a BLC lineage in cooperation with p63[46]. Together all these findings suggest a role for Yap-Myc-Trp63 in the acquisition of SCMC state whereas an increase in Taz or a lack of Yap-Myc-Trp63 promotes AT1 cell differentiation.

Interestingly, though we have long favored a role for Taz and not Yap in AT1 cell differentiation and maintenance, some reports seem to suggest a role for Yap in AT1 cell differentiation[59,60]. To definitively answer this question we generated *Sftpc*^{CreERT2};*Nf2*$^{f/f}$;*Wwtr1*$^{f/f}$;*mTmG* and *Sftpc*^{CreERT2};*Nf2*$^{f/f}$;*Yap1*$^{f/f}$;*mTmG* mice to investigate which nuclear effector of the Hippo pathway is required for the spontaneous differentiation of AT2 cells into AT1 cells upon *Nf2* inactivation. We now demonstrate that the simultaneous inactivation of *Nf2* and *Yap1* in AT2

https://doi.org/10.1038/s41467-024-54997-2

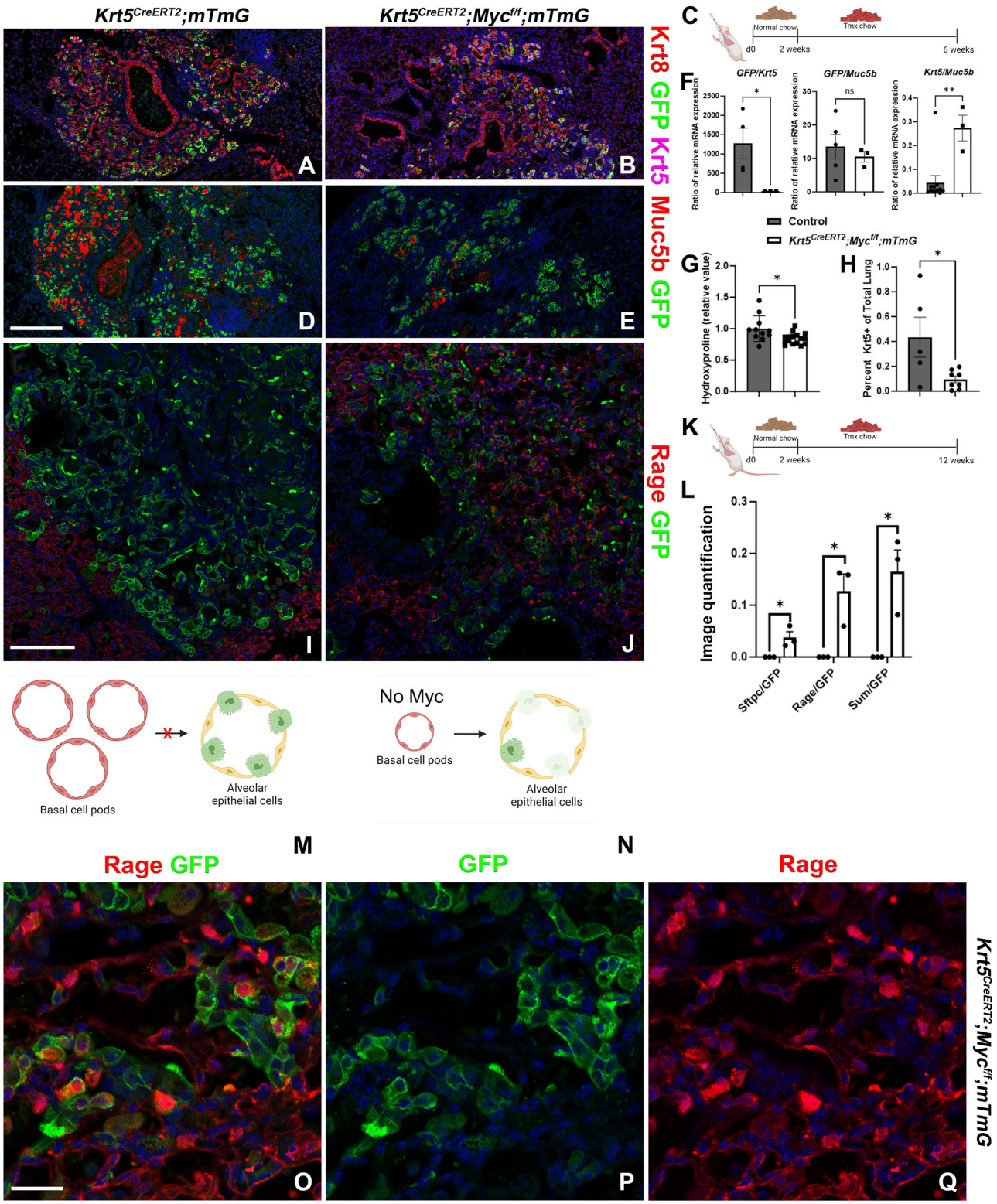

cells does not inhibit their spontaneous differentiation into AT1 cells (Fig. 8A–L, Q), whereas the simultaneous inactivation of *Nf2* and *Wwtr1* in AT2 cells completely blocks this process (Fig. 8A–Q).

If Taz promotes AT1 cell differentiation and Yap promotes BLC differentiation, inactivation of *Wwtr1* in bronchial epithelium using *Sox2*^{CreERT2}*;Wwtr1;mTmG* mice should mainly impair AT1 cell differentiation but not bronchiolization, whereas inactivation of *Yap1* in airways using *Sox2*^{CreERT2}*;Yap1*$^{f/f}$*;mTmG* mice should mainly impair bronchiolization. Interestingly, *Sox2*^{CreERT2}*;Wwtr1;mTmG* mice not only feature impaired AT1 cell differentiation but also increased bronchiolization (Fig. 7B, C, H, I, M, O). The latter is likely because Yap and Taz compete to bind to Tead transcription factors, with a loss of Taz resulting increased Yap/Tead binding. Vice versa, *Sox2*^{CreERT2}*;Yap1*$^{f/f}$*;mTmG* mice fail to generate BLCs and to bronchiolize the lung parenchyma upon severe bleomycin injury or H1N1 injury, with increased AT1 cell differentiation likely due to increased Taz/Tead, and increased pulmonary fibrosis as measured by hydroxyproline content as well as increased mortality (Fig. 7B, C, F, G, M, O & Supplementary Fig. 6A–I).

Fig. 5 | Myc drives basal cell pod expansion and maintenance after H1N1 injury. **C**, **K** *Krt5^{CreERT2};mTmG* and *Krt5^{CreERT2};Myc$^{f/f}$;mTmG* were infected with H1N1 at 8 weeks of age. At 2 weeks after injury, mice were placed on tamoxifen chow to inactivate *Myc* and permanently label all BLCs and their offspring with GFP and lungs were harvested at 6 (**A**-**H**) or 12 (**I**-**Q**) weeks post injury. **A**, **B** Coimmunostaining for Keratin 8 (Krt8; BLCs and transitional cells), GFP (lineage label), and Keratin5 (Krt5; basal and BLCs), (**D**, **E**) and coimmunostaining for Muc5b (mucus-producing secretory cells) and GFP (lineage label) on *Krt5^{CreERT2};mTmG* (**A**, **D**) and *Krt5^{CreERT2};Myc$^{f/f}$;mTmG* (**B**, **E**). **F** qPCR analysis for Gfp, *Krt5*, and *Muc5b Cre*- control ($n = 5$) and *Krt5^{CreERT2};Myc$^{f/f}$* ($n = 5$). Values are graphed as ratios (*GFP/Krt5* $p = 0.046$, *GFP/Muc5b* $p = 0.79$, *Krt5/Muc5b* $p = 0.006$). **G** Hydroxyproline analysis on *Cre*- control ($n = 10$) and *Krt5^{CreERT2};Myc$^{f/f}$* ($n = 16$) ($p = 0.01$). **H** Image analysis of total area of basal cells in influenza injured control (n = 6) and *Krt5^{CreERT2};Myc$^{f/f}$;mTmG* ($n = 8$) lung sections ($p = 0.02$). **I**, **J** Coimmunostaining for Rage (AT1 cells) and GFP (lineage label) on *Krt5^{CreERT2};mTmG* and *Krt5^{CreERT2};Myc$^{f/f}$;mTmG* lungs at 12 weeks post injury with magnification in **O**–**Q**. **L** Lineage tracing analysis on influenza injured lungs from immunostaining in **I** and (**J**) ($n = 3$). Area of GFP ($p = 0.02$), Sftpc ($p = 0.03$), and Rage ($p = 0.02$) were determined using Aivia machine learning software. **M**, **N** Diagram depicting that Myc deficient basal cells pods are smaller than Myc sufficient basal cell pods and can differentiating into Rage+ AT1 cells at 12 weeks after influenza injury. Created in BioRender. Warren. (2024) https://BioRender.com/ w28w946. Data are presented as mean values +/− SEM. Scale bars: 250 μm (**A**, **B**, **D**, **E**), 125 μm (**I**, **J**), 25 μm (**O**–**Q**). The two-tailed unpaired T-test was used to determine significance. *F* test was used to determine equal variances and unreported *F* values indicate equal variance. $^{*}p < 0.05$, $^{**}p < 0.01$.

Since overexpression of dominant active *Yap1^{S112A}* in BESCs is sufficient to drive Club cell to BLC differentiation[46], we wondered if overexpression of dominant active *Yap1^{S112A}* alone in BESCs and their offspring after bleomycin injury, using *Sox2^{CreERT2};LSL-rtTA;Tet-Yap1^{S112A}* mice, is sufficient to promote bronchiolization. Interestingly, while overexpression of a dominant active *Yap1^{S112A}* in BESCs is sufficient to drive BLC differentiation and prevent alveolar epithelial differentiation after bleomycin injury (Supplementary Fig. 6H–N), overexpression of dominant active *Yap1^{S112A}* did not induce *Myc* expression, and BESCs failed to acquire SCMC status and as such did not amplify nor invade the lung parenchyma nor destroy the remaining alveolar epithelium (Supplementary Fig. 6H–N).

This is interesting as we have just demonstrated that overexpression of *Myc* in Club cells after bleomycin injury causes them to acquire a super-competitor myoepithelial cell (SCMC) like status, coexpressing Krt5, Acta2, Sox9 and Myc (Fig. 6). Therefore, to specifically investigate the requirement for Yap and Myc in the acquisition of MEC-status we generated *Scgb1a1^{CreER};Yap1$^{f/f}$;LSL-rtTA;Tet-Myc* mice in which we could simultaneously inactivate *Yap1* and overexpress *Myc* in Club cells after bleomycin injury and found that BCs and MEC-like cells development was impaired, compared to *Scgb1a1^{CreER};LSL-rtTA;Tet-Myc* mice, indicating that both Myc and Yap are required for obtaining SCMC status (Fig. 6P).

Finally, to investigate if AT2 stem cells have the capacity to acquire a SCMC state and to bronchiolize the lung parenchyma we generated *Sftpc^{CreERT2};LSL-rtTA;Tet-Myc*, *Sftpc^{CreERT2};LSL-rtTA;Tet-Yap1^{S112A}* and *Sftpc^{CreERT2};LSL-rtTA;Tet-Myc;Tet-Yap1^{S112A}* mice in which we could respectively overexpress *Myc*, a dominant active *Yap1^{S112A}* or both in combination in AT2 stem cells and their progeny after bleomycin injury. We found that simultaneous overexpression of both *Myc* and *Yap1^{S112A}* in AT2 cells allowed them to adopt SCMC state and to bronchiolize the lung parenchyma (Supplementary Fig. 7A–D, M–O). However, overexpression of *Myc* or *Yap1^{S112A}* alone was not sufficient (Supplementary Fig. 7E-L).

Discussion

In this manuscript, we set out to investigate and clarify several unresolved issues on lung Hippo signaling, ARDS and pulmonary fibrosis. We find that different lung stem cell populations compete with one another to regenerate or remodel the lung and that this stem cell competition follows the classical cell competition model originally identified in *Drosophila*[61,62]. Our model in which bronchiolization of the lung parenchyma is reminiscent of the development of submucosal glands, has wide ranging implications for the early diagnosis of pulmonary fibrosis as well development of new treatments for this devastating disease. Especially, our findings about the distinct roles for Yap and Taz in bronchiolization vs alveolar epithelial regeneration will allow for the development of targeted therapies (Fig. 9).

It is thought that Yap and Myc coordinately regulate genes required for cell proliferation, where activation of Myc leads to extensive association with its genomic targets, most of which are prebound by TEAD[63]. At these loci, recruitment of Yap is thought to be Myc-dependent and required for full transcriptional activation. This cooperation between Yap and Myc is thought to be critical for cell cycle entry, organ growth, and tumorigenesis[63]. Cells can become super competitors through intrinsic (e.g., somatic mutations) or extrinsic mechanism[64]. At the molecular level, future studies will need to explore the impact of genetic perturbations on the ability of winner cells to contribute to cellular populations, both in vitro and in vivo. However, changes to gene expression shown to drive cell competition need not involve genetic engineering or mutations to the DNA itself. Cells may receive signals from their microenvironment, including cell-cell interactions, that converge on the cellular processor and drive cell competition behavior by affecting gene expression[65–67]. Similarly, epigenetic changes can also drive cell competition-relevant gene expression changes.

Under normal conditions, cell competition will select against the emergence of altered cells with disruptive behavior toward tissue integrity and/or tissue pattern formation. However, upon catastrophic organ injury this molecular machinery involved in the winner/loser interaction could be hijacked to maintain organism survival. In acute respiratory distress syndrome (ARDS), such as experienced after influenza or SARS-CoV-2 infection, the “dominant” stem cell populations (club cells and AT2 cells) are vulnerable to infection and normal alveolar tissue is steadily being replaced by bronchial/conducting airway epithelial cells which survive the infection but cannot participate in gas exchange. Stem cells in the conducting airway are sometimes considered a “reserve stem cell” population that only participates in alveolar epithelial repair after catastrophic injury to the lung parenchyma. As such, these “reserve stem” cells only win the fitness battle upon loss or destruction of alveolar type 2 (AT2) stem cells, considered the “dominant” stem cell population in the alveolar compartment[27]. We recently also reported increased bronchiolization in mice in which the fitness of AT2 cells was compromised[52]. Therefore, it appears that lowering AT2 stem cell fitness can be sufficient to cause conducting airway epithelial stem cells to acquire a competitive advantage and drive bronchiolization.

We demonstrate that active cell competition is a feature of pulmonary fibrosis/ARDS and its underlying mechanisms can be manipulated to help prevent and treat this disease. Lowering the fitness of BESCs can reduce and even reverse pulmonary fibrosis progression. Boosting the fitness/survival of AT2 stem cells or BASCs, could also prevent bronchiolization. Therefore, cell competition can be exploited to maximize the potential of healthy tissue replacement.

Methods

Experimental model and subject details

All mice were bred and maintained in a pathogen-free environment on a 12 hr light/dark cycle with free access to food and water. Ambient temperature was maintained at 21 °C–24 °C. Both male and female mice were used for all experiments. *Sox2^{CreERT2}* (JAX 017593; RRID:IMSR_JAX:017593), *Krt5^{CreERT2}* [68], *Scgb1a1^{CreERT}* (JAX 016225;

RRID:IMSR_JAX:016225), *Sftpc*^{CreERT2} [69], *Trp63*^{DreERT2} (Shanghai Model organisms Center NM-KI-190029; RRID:IMSR_NM-KI-190029), *Acta2*^{CreERT2} [70], *Sox9*^{CreERT2} (JAX 035092; RRID:IMS9R_JAX:035092), *mTmG* (JAX 007676; RRID:IMSR_JAX:007676), Rosa26-tdTomato (JAX 007909; RRID:IMSR_JAX:007909), RLTG (JAX 026931; RRID:IMSR_JAX:026931), FLTG (JAX 026932; RRID:IMSR_JAX:026932), *Stk3/4*$^{f/f}$ (JAX 017635; RRID:IMSR_JAX:017635), *Yap1*$^{f/f}$ [71], *Wwtr1*$^{f/f}$ [71], *Nf2*$^{f/f}$ [72], *Myc*$^{f/f}$ [73], *Rosa26-CAGs-LSL-rtTA3* (LSL-rtTA$^{f/f}$; JAX 029617;

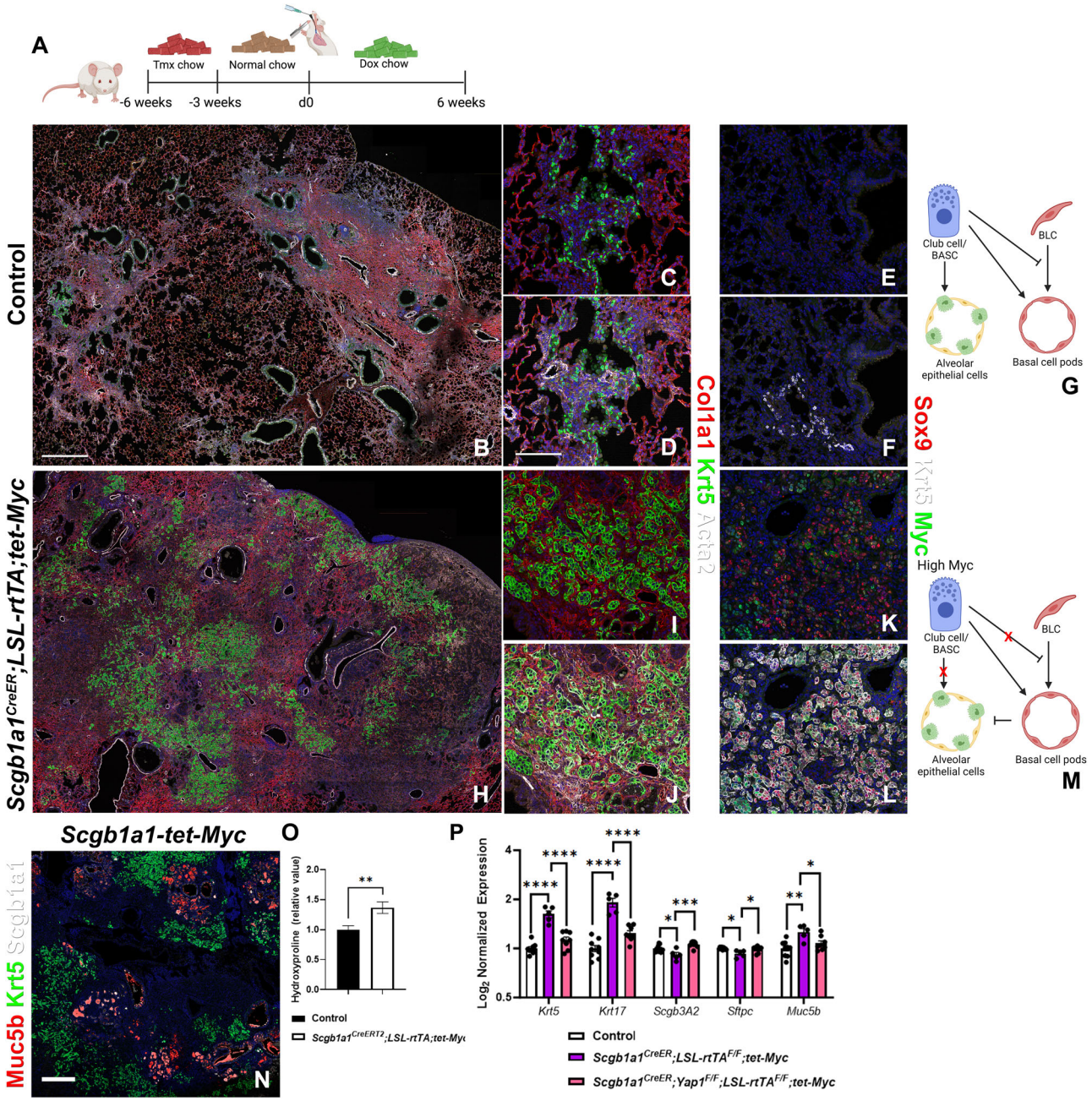

Fig. 6 | *Myc* overexpression in Club cells promotes SCMC status and bronchiolization. A Mice were placed on tamoxifen chow for 3 weeks and following a 3-week washout period, mice were injured with intratracheal administration of bleomycin and placed on doxycycline containing chow to induce *Myc* overexpression and harvested at 6 weeks post injury. **B**–**D**, **H**–**J** Coimmunostaining for markers associated with fibrosis and bronchiolization (Col1a1, Krt5, and Acta2) on control (**B**–**D**) and *Scgb1a1*^{CreERT}*;LSL-rtTA;Tet-Myc* (**H**–**J**). Coimmunostaining for myoepithelial cell-like markers Sox9, Krt5, and Myc on control (**E**, **F**) and *Scgb1a1*^{CreERT}*;LSL-rtTA;Tet-Myc* (**K**, **L**). **G**, **M** Diagram demonstrating that Myc sufficient Club cells inhibit basal cells and give rise to alveolar epithelial cells after bleomycin injury while Myc overexpressing Club cells dedifferentiate into basal cells and promote their invasion into the alveolus. Created in BioRender. Warren, R. (2024) https://BioRender.com/ l07p577. **N** Immunostaining for Muc5b (mucus producing secretory cells), Krt5 (BLCs), and Scgb1a1 (Club cells/BASCs) on *Scgb1a1*^{CreERT}*;LSL-rtTA;Tet-Myc*. **O** Hydroxyproline analysis on *Cre*- control ($n = 31$) and *Scgb1a1*^{CreERT}*;LSL-rtTA;Tet-Myc* ($n = 30$) normalized to control ($p = 0.003$). **P** Log2 normalized values for RNA expression for BLC (*Krt5, Krt17, Scgb3a2, Muc5b*) and AT2 cell (*Sftpc*) genes from NanoString analysis on control (n = 9 *Krt5* $p = 0.0000008$, *Krt17* $p = 0.000001$, *Scgb3a2* $p = 0.02$, *Sftpc* $p = 0.02$ F = 0.02, *Muc5b* $p = 0.002$), *Scgb1a1*^{CreERT}*;LSL-rtTA;Tet-Myc* ($n = 5$), and *Scgb1a1*^{CreERT}*;Yap*$^{f/f}$*;LSL-rtTA;Tet-Myc* ($n = 8$ *Krt5* $p = 0.0001$, *Krt17* $p = 0.00006$, *Scgb3a2* $p = 0.0007$, *Sftpc* $p = 0.04$,*Muc5b* $p = 0.02$). Values are normalized to control and p values are compared to *Scgb1a1*^{CreERT}*;LSL-rtTA;Tet-Myc*. Data are presented as mean values +/− SEM. Scale bars: 500 μm (**B**, **G**, **L**) and 100 μm (**C**–**F**, **H**–**K**). Two tailed unpaired T-test was used to determine significance. F test was used to determine equal variances and unreported F values indicate equal variance. *$p < 0.05$, **$p < 0.01$, ***$p < 0.001$, ****$p < 0.0001$.

https://doi.org/10.1038/s41467-024-54997-2

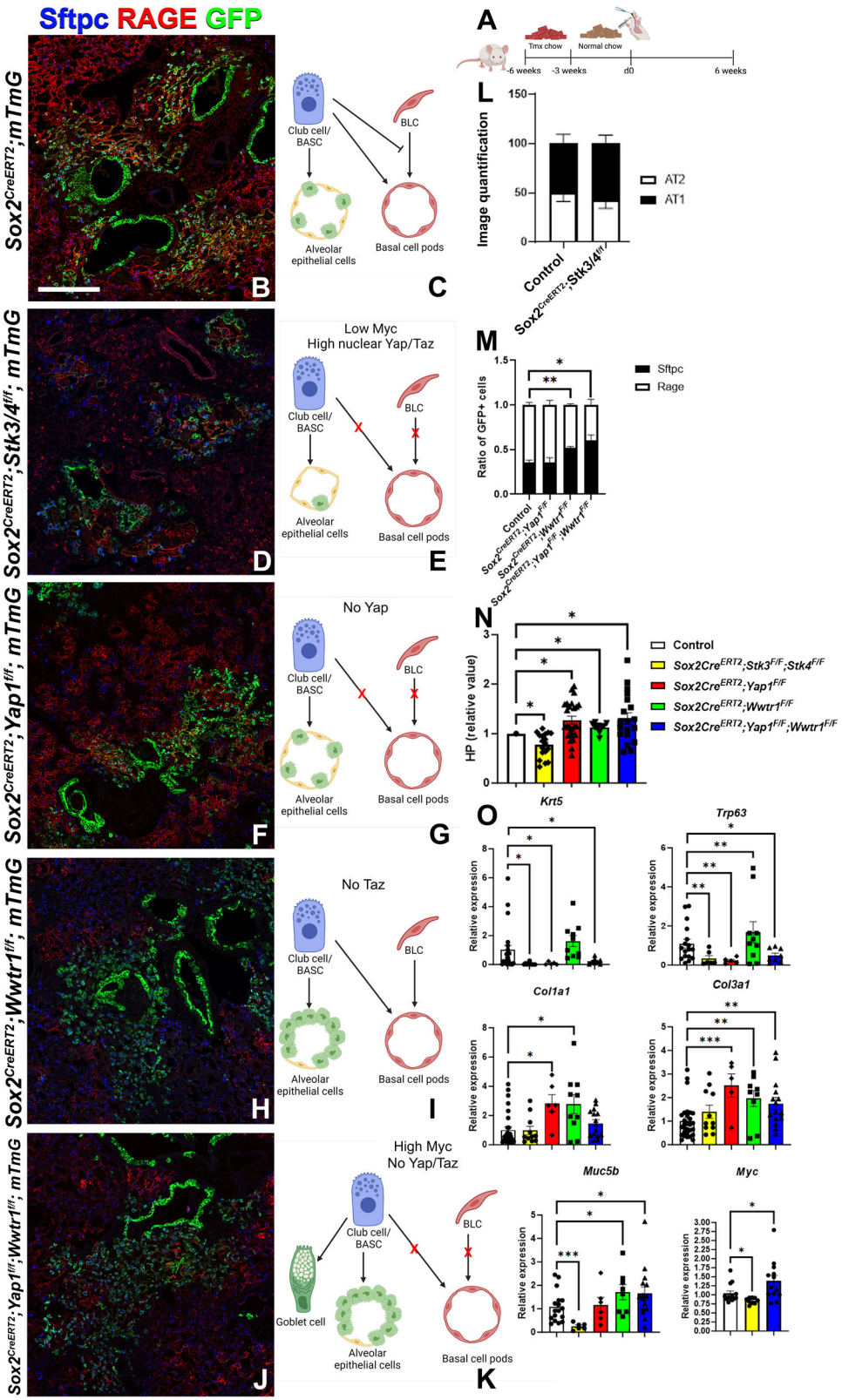

RRID:IMSR_JAX:029617), *Tet-Yap1-H2BGFP* (JAX 031279; RRID:IMSR_JAX:031279), *Tet-myc* (JAX 019376; RRID:IMSR_JAX:019376), *Acta2-Frt-STOP-Frt-CreERT2*[43], *Nkx2.1*^{Flpo} (JAX 028577; RRID:IMSR_JAX:028577) mice were previously described.

For bleomycin injury, adult 8- to 12-week-old mice were intratracheally instilled with 50 uL bleomycin (0.8–2 U/kg body weight optimized for each strain, batch of bleomycin, and gender) as described previously[74]. The following reagent was obtained through BEI Resources, NIAID, NIH: Influenza A Virus, A/Puerto Rico/8-9VMC3/1934 (H1N1), NR-29028. Mice were infected via intranasal route with a sublethal dose of H1N1 (100,000-162,500 viral forming units (VFU) optimized for each strain) diluted in 50 μL of saline. For tamoxifen induction, *Sftpc*^{CreERT2}, *Scgb1a1*^{CreER} and *Sox2*^{CreERT2} mice were placed on tamoxifen-containing chow (rodent diet with 400 mg/kg tamoxifen

Fig. 7 | Cytoplasmic Yap/Taz in airway epithelial cells inhibits bronchiolization and pulmonary fibrosis. A Mice were placed on tamoxifen chow for 3 weeks to inactivate *Yap1* and/or *Wwtr1* or *Stk3/4* and permanently label all Sox2+ cells and their offspring with GFP. Following a 3 week washout period, mice were injured with intratracheal administration of bleomycin and harvested at 6 weeks post injury. Coimmunostaining for Rage (AT1 cells), GFP (lineage label), and Sftpc (AT2 cells) on $Sox2^{CreERT2}$;*mTmG* (**B**), $Sox2^{CreERT2}$;$Stk3^{f/f}$;$Stk4^{f/f}$;*mTmG* (**D**), $Sox2^{CreERT2}$;$Yap1^{f/f}$;*mTmG* (**F**), $Sox2^{CreERT2}$;$Wwtr1^{f/f}$;*mTmG* (**H**), and $Sox2^{CreERT2}$;$Yap1^{f/f}$;$Wwtr1^{f/f}$;*mTmG* (**J**) lungs. **C**, **E**, **G**, **I**, **K** diagrams illustrating the direction of airway epithelial cell differentiation in figures (**B**, **D**, **F**, **H**, **J**). Created in BioRender. Warren (2024) https://BioRender.com/ a02e401. **L** Lineage tracing analysis on bleomycin injured lungs from immunostaining in B ($n = 3$) and **D** ($n = 4$) using Zeiss Zen Intellesis machine learning software to trace ($p = 0.57$). **M** Lineage tracing analysis on bleomycin-injured lungs from immunostaining in **B** ($n = 3$), **F** ($n = 5$, $p = 0.92$), **H** ($n = 4$, $p = 0.002$), and **J** ($n = 4$, $p = 0.004$) using Aivia machine learning software. **N** Hydroxyproline analysis on *Cre*- control, $Sox2^{CreERT2}$;$Yap1^{f/f}$;$Wwtr1^{f/f}$ ($n = 19$, $p = 0.04$), $Sox2^{CreERT2}$;$Yap1^{f/f}$ ($n = 25$, $p = 0.01$), $Sox2^{CreERT2}$;$Wwtr1^{f/f}$ ($n = 9$, $p = 0.04$), and $Sox2^{CreERT2}$;$Stk3^{f/f}$;$Stk4^{f/f}$ ($n = 18$, $p = 0.03$). **O** qPCR analysis for bronchiolization and fibrosis genes (*Krt5, p63, Col1a1, Col3a1* and *Muc5b*) on *Cre*- control ($n = 22$), $Sox2^{CreERT2}$;$Yap1^{f/f}$;$Wwtr1^{f/f}$ ($n = 8$, *Krt5* $p = 0.03$, $F = 0.00001$, *p63* $p = 0.03$, $F = 0.01$, *Col1a1* $p = 0.2$, *Col3a1* $p = 0.008$, and *Muc5b* $p = 0.05$), $Sox2^{CreERT2}$;$Yap1^{f/f}$ ($n = 5$, *Krt5* $p = 0.01$, $F = 0.00007$, *p63* $p = 0.002$, $F = 0.005$, *Col1a1* $p = 0.002$, *Col3a1* $p = 0.0005$ and *Muc5b* $p = 0.8$), $Sox2^{CreERT2}$;$Wwtr1^{f/f}$ ($n = 10$, *Krt5* $p = 0.27$, *p63* $p = 0.05$, *Col1a1* $p = 0.03$ $F = 0.02$, *Col3a1* $p = 0.004$ and *Muc5b* $p = 0.05$), and $Sox2^{CreERT2}$;$Stk3^{f/f}$;$Stk4^{f/f}$ ($n = 10$, *Krt5* $p = 0.009$, $F = 5.7 \times 10^{-8}$, *p63* $p = 0.01$ $F = 0.05$, *Col1a1* $p = 0.95$, *Col3a1* $p = 0.16$ and *Muc5b* $p = 0.00009$ $F = 0.003$). qPCR for *Myc* on control ($n = 23$), $Sox2^{CreERT2}$;$Yap1^{f/f}$;$Wwtr1^{f/f}$ ($n = 14$, $p = 0.05$) and $Sox2^{CreERT2}$;$Stk3^{f/f}$;$Stk4^{f/f}$ ($n = 10$, $p = 0.04$). Values are represented as $2^{-\Delta\Delta Ct}$ normalized to Control. Values are normalized to control. Data are presented as mean values +/− SEM. Scale bar: 200 μm. Two tailed unpaired T-test was used to determine significance. *F* test was used to determine equal variances and unreported *F* values indicate equal variance. $^{*}p < 0.05$, $^{**}p < 0.01$, $^{***}p < 0.001$.

citrate; Harlan Teklad TD.130860) for 3 weeks and $Sftpc^{CreERT2}$ and $Sox2^{CreERT2}$ mice received an additional intraperitoneal tamoxifen injection (0.20 mg/g body weight, Millipore Sigma) in the last week of tamoxifen citrate feed. Following a 3-week tamoxifen washout period, mice were either injured with bleomycin or H1N1. Mice containing *LSL-rtTA3* were placed on doxycycline containing chow (rodent diet with 625 mg/kg doxycycline; Harlan Teklad TD.09761) on the day of bleomycin. $Sox9^{CreERT2}$, $Trp63^{DreERT2}$;$Acta2^{CreERT2}$, and $Krt5^{CreERT2}$ mice were placed on tamoxifen containing chow beginning at 2 weeks following injury. All experiments were approved by the Mayo Clinic Institutional Animal Care and Use Committee.

Immunohistochemistry and fluorescence

All staining was done on paraffin sections of formalin-fixed lungs. Immunofluorescent staining was performed with the following primary antibodies: rabbit anti-Merlin (NF2; 1:250; clone A-19; sc-331; RRID:AB_2298548; Santa Cruz Biotechnology), rabbit anti-phospory-lated-Mst1(Thr183)/2(Thr180) (1:200; 3681; RRID:AB_330269; Cell Signaling Technologies), rabbit anti-phosphorylated Yap (Ser127) (1:200; 4911; RRID:AB_2218913; Cell Signaling Technologies), goat anti-Scgb1a1 (1:200; clone T-18; sc-9772; RRID:AB_2238819; Santa Cruz Biotechnology Inc.), goat anti-Sox9 (1:500; AF3075; RRID:AB_2194160; R&D Systems), mouse anti-Keratin 17 (1:50; clone Ks17.E3; sc-101461; RRID:AB_2234376; Santa Cruz Biotechnology, Inc.), chicken anti-GFP (1:500; GFP-1020; RRID:AB_10000240; Aves Labs Inc.), rabbit anti-Keratin 5 (1:200; clone EP1601Y; MA5-14473; RRID:AB_10979451; Thermo Fisher Scientific), chicken anti-Keratin 5 (1:500; 905901; RRID:AB_2565054; BioLegend), rabbit anti-SFTPC (1:200; WRAB-9337; RRID:AB_2335890; Seven hills bioreagents), rat anti-RAGE (1:500; Clone 175410; MAB1179; RRID:AB_2289349; R&D Systems), goat anti-RAGE (1:500; AF1145; RRID:AB_354628; R&D Systems), rat anti-Keratin 8 (1:100; TROMA-I; RRID:AB_531826; Developmental Studies Hybridoma Bank), Syrian hamster anti-podoplanin (PDPN, T1a; 1:500; 8.1.1; RRID:AB_531893; Developmental Studies Hybridoma Bank), rabbit anti-mucin 5b (Muc5b; 1:250; clone H-300; sc-20119; RRID:AB_2282256; Santa Cruz Biotechnology Inc.), mouse anti-alpha actin (smooth muscle actin (SMA), Acta2; 1:500; Clone 1A4; sc-32251; RRID:AB_262054; Santa Cruz Biotechnology Inc.), rabbit anti-myc (1:200; clone Y69, ab32072; RRID:AB_731658; Abcam), rabbit anti-human Myc (1:200; clone C-19; sc-788; RRID:AB_631277), rabbit anti-collagen I (1:500; ab34710; RRID:AB_731684; Abcam), mouse anti−beta-tubulin (1:500; clone 3F3-G2; LMAB-3F3; RRID:AB_451728; Seven Hills Bioreagents), and rabbit anti-p63 (1:500; clone poly6190; 619002; RRID:AB_2207170; BioLegend).

After deparaffinization, slides were rehydrated through a series of decreasing ethanol concentrations, antigen unmasked by either microwaving in citrate-based antigen unmasking solution (Vector Labs, H-3300) or by incubating sections with proteinase K (7.5 μg/ml) (Invitrogen, 25530-049) for 7 min at 37 °C. Tissue sections were then washed in TBS with 0.1% Tween-20 and blocked with 3% Bovine Serum Albumin (BSA), 0.4% Triton X-100 in TBS for 30 min at room temperature followed by overnight incubation of primary antibodies diluted in 3% BSA, 0.1% Triton X-100 in TBS. The next day, slides were washed in TBS with 0.1% Tween-20 and incubated with secondary antibodies diluted in 3% BSA, 0.1% Triton X-100 in TBS for 3 h at room temperature. All fluorescent staining was performed with appropriate secondary antibodies from Jackson Immunoresearch. Slides were mounted using Vectashield (Vector Labs, H-1000).

Microscopy and imaging

Tissue was imaged using a micrometer slide calibrated Zeiss LSM800 Laser scanning confocal microscope using ZEN imaging software or Leica Stellaris 5 confocal microscope with LASX imaging software. Lungs were imaged using tiled stitched 20x images covering the entire cross-section of the left or lower right lung lobe from ≥6 different lungs. Representative images were chosen. Images were processed and analyzed using Zen blue (Zeiss), LASX (Leica), and Adobe Photoshop 2024 (Adobe) software.

Image quantification

Differentiation of GFP-positive cells was determined using machine learning and machine learning image segmentation with Aivia software. The total area of GFP and GFP overlapping with different cell-specific antibody stains (Sftpc or RAGE) was determined. Image quantification and analysis were performed in a double-blinded fashion. Each quantification was ≥3 different mouse lungs.

Quantitative real-time PCR

Total mRNA was extracted from lung accessory lobes stored in RNA-Later (Invitrogen, AM7021) and using Total RNA Kit I (Omega Biotek, R6834-02) according to the manufacturer's instructions. RNA concentration was determined by spectrophotometry. cDNA was generated using Maxima™ First Strand cDNA Synthesis (Fisher Scientific, FERK1642) according to the manufacturer's instructions. Gene expression was analyzed by quantitative RT-PCR using Taqman Gene Expression Assays (Applied Biosystems, 4369016) directed against the mouse targets *β-glucuronidase* (Mm00446953_m1), *Krt5* (Mm01305291_g1), *Trp63* (Mm00495788_m1), *Muc5b* (Mm00466391_m1), *Col1a1* (Mm00801666_g1), *Col3a1* (Mm01254476_m1), *Myc* (Mm00487803_m1). Quantitative real-time PCR was performed using a StepOne Plus system (Applied Biosystems). Data were presented as $2^{-\Delta\Delta Ct}$ with *β-glucuronidase* as the internal sample control normalized to control group. Each experiment was repeated with samples obtained from ≥3 different lung preparations.

https://doi.org/10.1038/s41467-024-54997-2

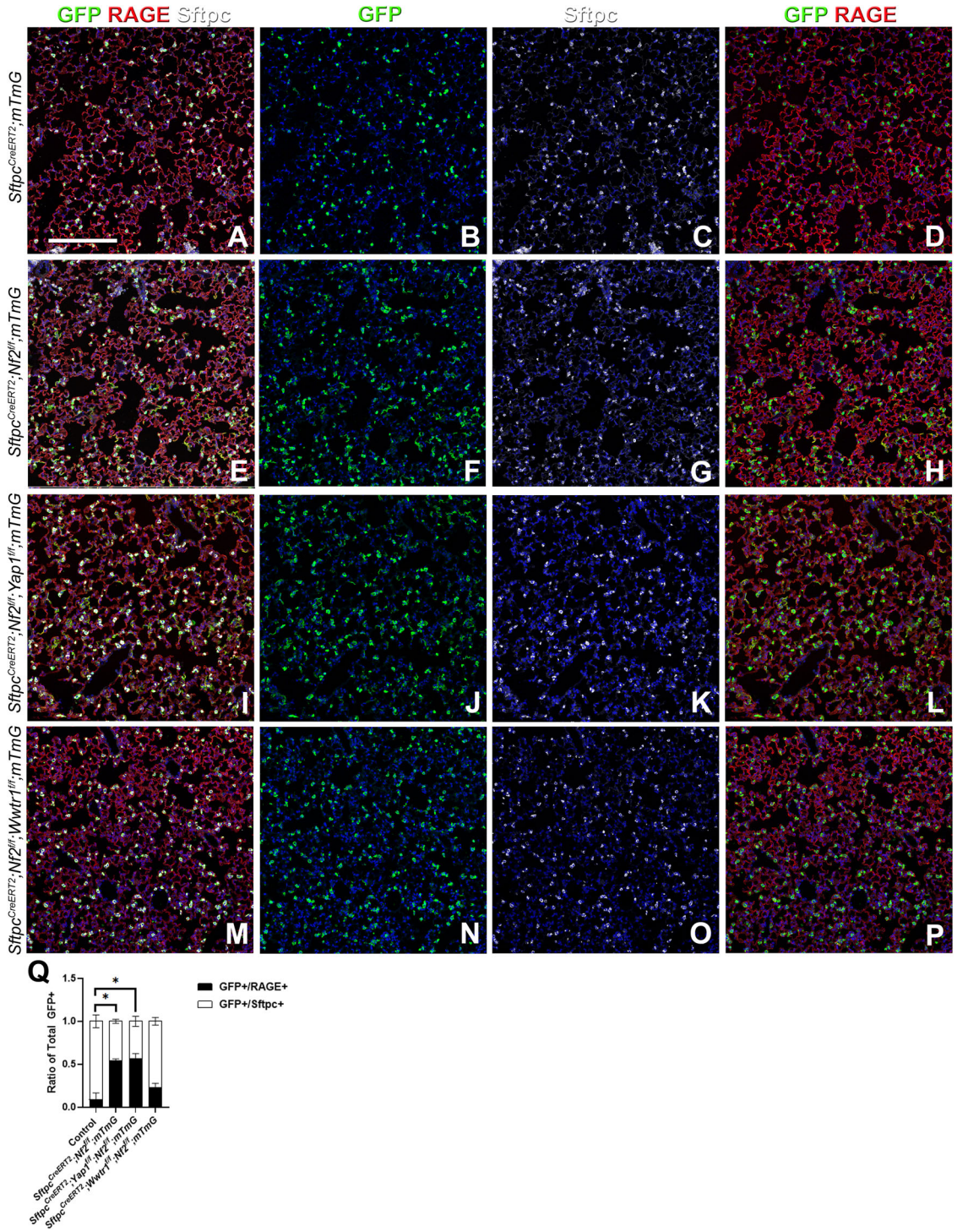

Fig. 8 | Taz is required for AT1 cell differentiation. A–P *Sftpc*^{CreERT2}*;mTmG*, *Sftpc*^{CreERT2}*;Nf2*$^{f/f}$*;mTmG*, *Sftpc*^{CreERT2}*;Nf2*$^{f/f}$*;Yap1*$^{f/f}$*;mTmG*, and *Sftpc*^{CreERT2}*;Nf2*$^{f/f}$*;Wwtr1*$^{f/f}$*;mTmG* were placed on tamoxifen containing chow at 8 weeks of age for 3 weeks to inactivate *Nf2* and/or *Yap1* and/or *Wwtr1* and permanently lineage label AT2 stem cells and their offspring. At 9 weeks after being placed on normal chow left lung lobes were inflation fixed, embedded in paraffin, and sectioned. Coimmunostaining for GFP (lineage label), Rage (AT1 cells), and Sftpc (AT2 cells). **Q** Image analysis for lineage labeled AT1 and AT2 cells in A-P using Aivia machine learning software (*Sftpc*^{CreERT2}*;mTmG* (n = 6), *Sftpc*^{CreERT2}*;Nf2*$^{f/f}$*;mTmG* ($n = 8$, p = 0.00003), *Sftpc*^{CreERT2}*;Nf2*$^{f/f}$*;Yap1*$^{f/f}$*;mTmG* ($n = 5$, $p = 0.0009$), and *Sftpc*^{CreERT2}*;Nf2*$^{f/f}$*;Wwtr1*$^{f/f}$*;mTmG* ($n = 6$, $p = 0.13$)). Data are presented as mean values +/− SEM. Two tailed unpaired T-test was used to determine significance. F test was used to determine equal variances. Scale bar: 200µm. $^{*}p < 0.05$.

Nanostring

RNA was isolated from lung accessory lobes as described above. 100 ng of RNA was hybridized with a custom RNA probe panel designed by NanoString (NanoString Technologies; DL_1206_C9662) for 16 hours according to manufacturer's instructions. The RNA-probe hybridization was loaded on a NanoString cartridge and processed in a NanoString nCounter. Data was analyzed with Rosalind.bio (Rosalind, Inc) and Log2 Fold Changes were calculated and graphed. Each experiment was repeated with samples obtained from ≥3 different lung preparations.

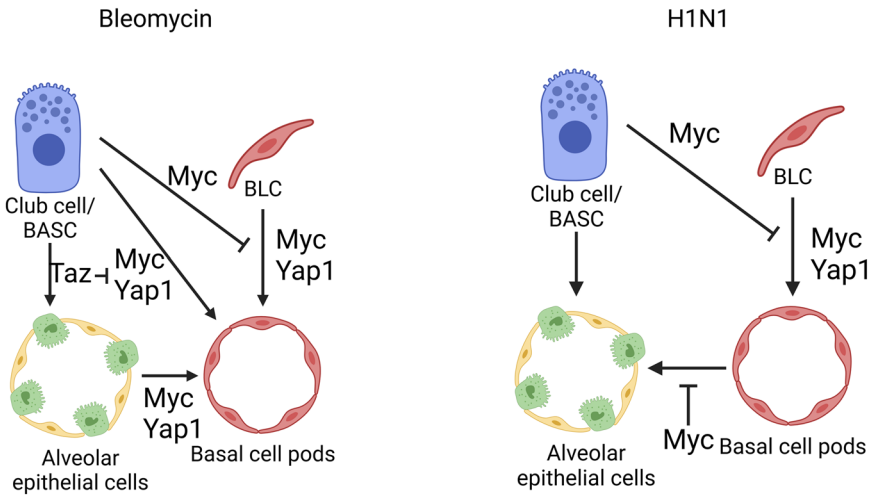

Fig. 9 | Myc and Yap1 increase stem cell competitiveness to drive bronchiolization. Stem cells exhibiting the highest Myc and Yap1 levels become super-competitors that drive remodeling, whereas Taz promotes terminal differentiation into AT1 cells by inhibiting Myc. *Created in BioRender. Warren, R. (2024)* https://BioRender.com/d35d050.

Human subjects and sample acquisition

Explant tissue was obtained from patients undergoing transplantation for end-stage IPF, fixed and paraffin-embedded in compliance with consent procedures accepted by the Internal Review Board at Mayo Clinic.

Single cell RNA sequencing of Human IPF tissue

Epithelial cells from donor distal samples and IPF fibrotic samples were subsets from GSE132914 for this analysis[75]. Standard data integration workflow from the Seurat V3 package was applied to integrate and combine data sets for unsupervised clustering. The batch correction was processed with PCA (Principal Component Analysis) using the 5000 most variable genes, and the first 30 independent components were used for downstream unbiased clustering with a resolution of 0.4. The UMAP (Uniform Manifold Approximation and Projection) method was used for visualization of unsupervised clustering and basal cell subset with the first 30 independent PCA components. The cell type of each cluster is determined by known markers of individual cell types. Gene expression levels were shown using the FeaturePlot function from the Seurat Package.

Spatial transcriptomics

RNA was isolated from formalin fixed paraffin-embedded (FFPE) tissue sections using E.Z.N.A FFPE RNA Kit (Omega Bio-Tek). The RNA integrity in FFPE blocks was determined on an Agilent TapeStation. 5μm FFPE lung sections that had a DV200% above 50 were placed within the frames of the capture areas on the active surface of the Visium spatial slide (10x Genomics) and processed according to manufacturer's instructions. Tissues were stained with podoplanin (PDPN, T1a) and GFP and imaged with fluorescent secondary antibodies. Final library preparations and sequencing were completed by the Mayo Genomics Research Core according to manufacturer's instructions on an Illumina NextSeq. Count matrices were generated using the 'spaceranger count' function in Space Ranger 1.0.0. The resulting data were processed in Scanpy and Squidpy.

Hydroxyproline

The right lobes were flash-frozen in dry ice at the time of harvest and stored at −80 °C. For acid hydrolysis, the lobes were baked in a 70 °C oven without lids for 2 days until completely dry. The weights of dry lobes were measured and 500 μl of 6 N HCl were added to each sample. The lungs were then hydrolyzed in an 85 °C oven for 2 days with occasional vortexing. The hydrolysates were cooled at room temperature and centrifuged at maximum speed for 10 minutes. The supernatants then were transferred to fresh 1.5 mL tubes and centrifuged at maximum speed for 10 minutes. Each sample or standard was diluted with citrate-acetate buffer (5% citric acid, 1.2% glacial acetic acid, 7.24% sodium acetate, and 3.4% sodium hydroxide) in a 96-well plate. Chloramine-T solution (1.4% chloramine-T, 10% N-propanol, and 80% citrate-acetate buffer) was added, and the mixture was incubated for 20 minutes at room temperature. Then, Ehrlich's solution (1.27 M p-dimethylaminobenzaldehyde, 70% N-propanol, 20% perchloric acid) was added to each sample and the samples were incubated at 65 °C for 20 minutes. Absorbance was measured at 550 nm. Standard curves were generated for each experiment using the reagent hydroxyproline (Sigma H-1637) as a standard. The amount (μg) of hydroxyproline were calculated by comparison to the standard curve.

Statistics and reproducibility

All results are expressed as mean values ± SEM. The 'n' represents biological replicates and can be found in the figure legends. The significance of differences between 2 sample means was determined by two-tailed unpaired T-test (assuming unequal or equal variances as determined by the F-test of equality of variances). All datasets followed a normal distribution and P values less than 0.05 were considered statistically significant. The number of samples to be used was based on the number of experimental paradigms multiplied by the number in each group that is necessary to yield statistically significant results (based on power analysis, to reject the null hypothesis with 80% power (type I error = 0.05).

Reporting summary

Further information on research design is available in the Nature Portfolio Reporting Summary linked to this article.

Data availability

Epithelial cells from donor proximal and distal samples and IPF fibrotic samples were subset from GSE132914. 10x Genomics Visium Spatial Transcriptomics generated in this study have been deposited in the GEO Repository under GSE282002. Further information and requests for resources and reagents should be directed to and will be fulfilled by

the Lead Contact, Stijn De Langhe: delanghe.stijn@mayo.edu. Source data are provided with this paper.

References

1. Barkauskas, C. E. & Noble, P. W. Cellular mechanisms of tissue fibrosis. 7. New insights into the cellular mechanisms of pulmonary fibrosis. *Am. J. Physiol. Cell Physiol.* **306**, C987–C996 (2014).
2. King, T. E. Jr., Pardo, A. & Selman, M. Idiopathic pulmonary fibrosis. *Lancet* **378**, 1949–1961 (2011).
3. Steele, M. P. & Schwartz, D. A. Molecular mechanisms in progressive idiopathic pulmonary fibrosis. *Annu. Rev. Med.* **64**, 265–276 (2013).
4. Parimon, T., Yao, C., Stripp, B. R., Noble, P. W. & Chen, P. Alveolar Epithelial Type II cells as drivers of lung fibrosis in idiopathic pulmonary fibrosis. *Int J. Mol. Sci.* **21**, 2269 (2020).
5. Dressen, A. et al. Analysis of protein-altering variants in telomerase genes and their association with MUC5B common variant status in patients with idiopathic pulmonary fibrosis: a candidate gene sequencing study. *Lancet Respir. Med.* **6**, 603–614 (2018).
6. Allen, R. J. et al. Genome-wide association study of susceptibility to idiopathic pulmonary fibrosis. *Am. J. Respir. Crit. Care Med.* **201**, 564–574 (2020).
7. Winters, N. I., Burman, A., Kropski, J. A. & Blackwell, T. S. Epithelial injury and dysfunction in the pathogenesis of idiopathic pulmonary fibrosis. *Am. J. Med Sci.* **357**, 374–378 (2019).
8. Povedano, J. M. et al. Therapeutic effects of telomerase in mice with pulmonary fibrosis induced by damage to the lungs and short telomeres. *Elife* **7**, e31299 (2018).
9. Strunz, M. et al. Alveolar regeneration through a Krt8+ transitional stem cell state that persists in human lung fibrosis. *Nat. Commun.* **11**, 3559 (2020).
10. Kobayashi, Y. et al. Persistence of a regeneration-associated, transitional alveolar epithelial cell state in pulmonary fibrosis. *Nat. Cell Biol.* **22**, 934–946 (2020).
11. Kadur Lakshminarasimha Murthy, P. et al. Human distal lung maps and lineage hierarchies reveal a bipotent progenitor. *Nature* **604**, 111–119 (2022).
12. Adams, T. S. et al. Single-cell RNA-seq reveals ectopic and aberrant lung-resident cell populations in idiopathic pulmonary fibrosis. *Sci. Adv.* **6**, eaba1983 (2020).
13. Ray, S. et al. Rare SOX2(+) airway progenitor cells generate KRT5(+) cells that repopulate damaged alveolar parenchyma following influenza virus infection. *Stem Cell Rep.* **7**, 817–825 (2016).
14. Yang, Y. et al. Spatial-temporal lineage restrictions of embryonic p63(+) progenitors establish distinct stem cell pools in adult airways. *Dev. Cell* **44**, 752–761.e754 (2018).
15. Kumar, P. A. et al. Distal airway stem cells yield alveoli in vitro and during lung regeneration following H1N1 influenza infection. *Cell* **147**, 525–538 (2011).
16. Xi, Y. et al. Local lung hypoxia determines epithelial fate decisions during alveolar regeneration. *Nat. Cell Biol.* **19**, 904–914 (2017).
17. Redente, E. F. et al. Persistent, progressive pulmonary fibrosis and epithelial remodeling in mice. *Am. J. Respir. Cell Mol. Biol.* **64**, 669–676 (2021).
18. Seibold, M. A. et al. The idiopathic pulmonary fibrosis honeycomb cyst contains a mucocilary pseudostratified epithelium. *PLoS One* **8**, e58658 (2013).
19. Jiang, P. et al. Ineffectual Type 2-to-Type 1 alveolar epithelial cell differentiation in idiopathic pulmonary fibrosis: persistence of the KRT8(hi) transitional state. *Am. J. Respir. Crit. Care Med.* **201**, 1443–1447 (2020).
20. Yuan, T. et al. FGF10-FGFR2B signaling generates basal cells and drives alveolar epithelial regeneration by bronchial epithelial stem cells after lung injury. *Stem Cell Rep.* **12**, 1041–1055 (2019).
21. Vaughan, A. E. et al. Lineage-negative progenitors mobilize to regenerate lung epithelium after major injury. *Nature* **517**, 621–625 (2015).
22. Beppu, A. K. et al. Epithelial plasticity and innate immune activation promote lung tissue remodeling following respiratory viral infection. *Nat. Commun.* **14**, 5814 (2023).
23. Zuo, W. et al. p63(+)Krt5(+) distal airway stem cells are essential for lung regeneration. *Nature* **517**, 616–620 (2015).
24. Weiner, A. I. et al. DeltaNp63 drives dysplastic alveolar remodeling and restricts epithelial plasticity upon severe lung injury. *Cell Rep.* **41**, 111805 (2022).
25. Wu, C. T. et al. SARS-CoV-2 replication in airway epithelia requires motile cilia and microvillar reprogramming. *Cell* **186**, 112–130 e120 (2023).
26. Garcia, G. L., Valenzuela, A., Manzoni, T., Vaughan, A. E. & Lopez, C. B. Distinct chronic post-viral lung diseases upon infection with influenza or parainfluenza viruses differentially impact superinfection outcome. *Am. J. Pathol.* **190**, 543–553 (2020).
27. Hernandez, B. J. et al. Intermediary role of lung alveolar Type 1 cells in epithelial repair upon sendai virus infection. *Am. J. Respir. Cell Mol. Biol.* **67**, 389–401 (2022).
28. Baker, N. E. Emerging mechanisms of cell competition. *Nat. Rev. Genet.* **21**, 683–697 (2020).
29. Claveria, C., Giovinazzo, G., Sierra, R. & Torres, M. Myc-driven endogenous cell competition in the early mammalian embryo. *Nature* **500**, 39–44 (2013).
30. Sancho, M. et al. Competitive interactions eliminate unfit embryonic stem cells at the onset of differentiation. *Dev. Cell* **26**, 19–30 (2013).
31. Vincent, J. P., Fletcher, A. G. & Baena-Lopez, L. A. Mechanisms and mechanics of cell competition in epithelia. *Nat. Rev. Mol. Cell Biol.* **14**, 581–591 (2013).
32. Madan, E. et al. Flower isoforms promote competitive growth in cancer. *Nature* **572**, 260–264 (2019).
33. Pelham, C. J., Nagane, M. & Madan, E. Cell competition in tumor evolution and heterogeneity: Merging past and present. *Semin Cancer Biol.* **63**, 11–18 (2020).
34. Nagata, R. & Igaki, T. Cell competition: Emerging mechanisms to eliminate neighbors. *Dev. Growth Differ.* **60**, 522–530 (2018).
35. Bowling, S., Lawlor, K. & Rodriguez, T. A. Cell competition: the winners and losers of fitness selection. *Development* **146**, dev167486 (2019).
36. De la Cova, C., Abril, M., Bellosta, P., Gallant, P. & Johnston, L. A. Drosophila myc regulates organ size by inducing cell competition. *Cell* **117**, 107–116 (2004).
37. Moreno, E. & Basler, K. dMyc transforms cells into supercompetitors. *Cell* **117**, 117–129 (2004).
38. Zheng, D. et al. A cellular pathway involved in Clara cell to alveolar type II cell differentiation after severe lung injury. *PLoS One* **8**, e71028 (2013).
39. Zheng, D. et al. Regeneration of alveolar type I and II cells from Scgb1a1-expressing cells following severe pulmonary damage induced by bleomycin and influenza. *PLoS One* **7**, e48451 (2012).
40. Barkauskas, C. E. et al. Type 2 alveolar cells are stem cells in adult lung. *J. Clin. Invest* **123**, 3025–3036 (2013).
41. Volckaert, T. & De Langhe, S. Lung epithelial stem cells and their niches: Fgf10 takes center stage. *Fibrogenes. Tissue Repair* **7**, 8 (2014).
42. Fernanda de Mello Costa, M., Weiner, A. I. & Vaughan, A. E. Basal-like progenitor cells: a review of dysplastic alveolar regeneration and remodeling in lung repair. *Stem Cell Rep.* **15**, 1015–1025 (2020).
43. Lyu, H. et al. Niche-mediated repair of airways is directed in an occupant-dependent manner. *Cell Rep.* **41**, 111863 (2022).

44. Engelhardt, J. F., Schlossberg, H., Yankaskas, J. R. & Dudus, L. Progenitor cells of the adult human airway involved in submucosal gland development. *Development* **121**, 2031–2046 (1995).
45. Anderson, P. J., Lynch, T. J. & Engelhardt, J. F. Multipotent myoepithelial progenitor cells are born early during airway submucosal gland development. *Am. J. Respir. Cell Mol. Biol.* **56**, 716–726 (2017).
46. Zhao, R. et al. Yap tunes airway epithelial size and architecture by regulating the identity, maintenance, and self-renewal of stem cells. *Dev. Cell* **30**, 151–165 (2014).
47. Song, H. et al. Mammalian Mst1 and Mst2 kinases play essential roles in organ size control and tumor suppression. *Proc. Natl Acad. Sci. USA* **107**, 1431–1436 (2010).
48. Lee, K. P. et al. The Hippo-Salvador pathway restrains hepatic oval cell proliferation, liver size, and liver tumorigenesis. *Proc. Natl Acad. Sci. USA* **107**, 8248–8253 (2010).
49. He, T. C. et al. Identification of c-MYC as a target of the APC pathway. *Science* **281**, 1509–1512 (1998).
50. Azzolin, L. et al. YAP/TAZ incorporation in the beta-catenin destruction complex orchestrates the Wnt response. *Cell* **158**, 157–170 (2014).
51. Varelas, X. et al. The Hippo pathway regulates Wnt/beta-catenin signaling. *Dev. Cell* **18**, 579–591 (2010).
52. Warren R., Lyu H., Klinkhammer K. & De Langhe S. P. Hippo signaling impairs alveolar epithelial regeneration in pulmonary fibrosis. *Elife* **12**, https://doi.org/10.7554/eLife.85092 (2023).
53. Gokey, J. J. et al. Active epithelial Hippo signaling in idiopathic pulmonary fibrosis. *JCI Insight* **3**, e98738 (2018).
54. Xu, Y. et al. Single-cell RNA sequencing identifies diverse roles of epithelial cells in idiopathic pulmonary fibrosis. *JCI Insight* **1**, e90558 (2016).
55. Hicks-Berthet, J. et al. Yap/Taz inhibit goblet cell fate to maintain lung epithelial homeostasis. *Cell Rep.* **36**, 109347 (2021).
56. Mucenski, M. L. et al. Beta-catenin regulates differentiation of respiratory epithelial cells in vivo. *Am. J. Physiol. Lung Cell Mol. Physiol.* **289**, L971–L979 (2005).
57. Jeon, H. Y. et al. Airway secretory cell fate conversion via YAP-mTORC1-dependent essential amino acid metabolism. *EMBO J.* **41**, e109365 (2022).
58. Volckaert, T. et al. Fgf10-Hippo Epithelial-mesenchymal crosstalk maintains and recruits lung basal stem cells. *Dev. Cell* **43**, 48–59 e45 (2017).
59. Penkala, I. J. et al. Age-dependent alveolar epithelial plasticity orchestrates lung homeostasis and regeneration. *Cell Stem Cell* **28**, 1775–1789 e1775 (2021).
60. Burgess, C. L. et al. Generation of human alveolar epithelial type I cells from pluripotent stem cells. *Cell Stem Cell* **31**, 657–675 e658 (2024).
61. Morata, G. & Ripoll, P. Minutes: mutants of drosophila autonomously affecting cell division rate. *Dev. Biol.* **42**, 211–221 (1975).
62. Simpson, P. & Morata, G. Differential mitotic rates and patterns of growth in compartments in the Drosophila wing. *Dev. Biol.* **85**, 299–308 (1981).
63. Croci, O. et al. Transcriptional integration of mitogenic and mechanical signals by Myc and YAP. *Genes Dev.* **31**, 2017–2022 (2017).
64. Fowler, J. C. & Jones, P. H. Somatic mutation: what shapes the mutational landscape of normal epithelia? *Cancer Discov.* **12**, 1642–1655 (2022).
65. Maheden, K., Bashth, O. S. & Shakiba, N. Evening the playing field: microenvironmental control over stem cell competition during fate programming. *Curr. Opin. Genet Dev.* **70**, 66–75 (2021).
66. Maheden, K., Zhang, V. W. & Shakiba, N. The field of cell competition comes of age: semantics and technological synergy. *Front Cell Dev. Biol.* **10**, 891569 (2022).
67. Shakiba, N., Jones, R. D., Weiss, R. & Del Vecchio, D. Context-aware synthetic biology by controller design: Engineering the mammalian cell. *Cell Syst.* **12**, 561–592 (2021).
68. Van Keymeulen, A. et al. Distinct stem cells contribute to mammary gland development and maintenance. *Nature* **479**, 189–193 (2011).
69. Chapman, H. A. et al. Integrin alpha6beta4 identifies an adult distal lung epithelial population with regenerative potential in mice. *J. Clin. Invest.* **121**, 2855–2862 (2011).
70. Wendling, O., Bornert, J. M., Chambon, P. & Metzger, D. Efficient temporally-controlled targeted mutagenesis in smooth muscle cells of the adult mouse. *Genesis* **47**, 14–18 (2009).
71. Xin, M. et al. Hippo pathway effector Yap promotes cardiac regeneration. *Proc. Natl Acad. Sci. USA* **110**, 13839–13844 (2013).
72. Giovannini, M. et al. Conditional biallelic Nf2 mutation in the mouse promotes manifestations of human neurofibromatosis type 2. *Genes Dev.* **14**, 1617–1630 (2000).
73. Trumpp, A. et al. c-Myc regulates mammalian body size by controlling cell number but not cell size. *Nature* **414**, 768–773 (2001).
74. Redente, E. F. et al. Tumor necrosis factor-alpha accelerates the resolution of established pulmonary fibrosis in mice by targeting profibrotic lung macrophages. *Am. J. Respir. Cell Mol. Biol.* **50**, 825–837 (2014).
75. Yao, C. et al. Senescence of alveolar Type 2 cells drives progressive pulmonary fibrosis. *Am. J. Respir. Crit. Care Med.* **203**, 707–717 (2021).

Acknowledgements

This study was supported by NIH R01 HL146461 (S.D.L), HL132156 (S.D.L), NIH R35 HL161169 (S.D.L.) NIH T32 HL105355 (R.W.) and Mayo Clinic Brewer Family Career Development Award (R.W).

Author contributions

R.W. designed and performed experiments, interpreted the data, and prepared the manuscript. K.K., H.L., J.K., and T.Y. performed experiments. C.Y. and B.S. performed and analyzed single-cell sequencing data. S.P.D-L conceived, designed, and supervised the study, analyze the data, and prepared the manuscript.

Competing interests

The authors declare no competing interests.

Additional information

Supplementary information The online version contains supplementary material available at https://doi.org/10.1038/s41467-024-54997-2.

Correspondence and requests for materials should be addressed to Stijn P. De Langhe.

Peer review information *Nature Communications* thanks Tien Peng, and the other, anonymous, reviewer(s) for their contribution to the peer review of this work. A peer review file is available.